cmgh
CELLULAR AND MOLECULAR GASTROENTEROLOGY AND HEPATOLOGY

ORIGINAL RESEARCH

Increased Pancreatic Protease Activity in Response to Antibiotics Impairs Gut Barrier and Triggers Colitis

Hongsup Yoon,[1] Monika Schaubeck,[2] Ilias Lagkouvardos,[3,4] Andreas Blesl,[5] Stephanie Heinzlmeir,[6,7] Hannes Hahne,[6,8] Thomas Clavel,[4,9] Suchita Panda,[10] Christina Ludwig,[7] Bernhard Kuster,[6,7] Chaysavanh Manichanh,[10] Patrizia Kump,[5] Dirk Haller,[1,4,*] and Gabriele Hörmannsperger[1,*]

[1]Technische Universität München, Chair of Nutrition and Immunology, Freising-Weihenstephan, Germany; [2]Max Planck Institute of Neurobiology, Department of Neuroimmunology, Martinsried, Germany; [3]Technische Universität München, Junior Research Group Microbial Bioinformatics, ZIEL – Institute for Food and Health, Freising-Weihenstephan, Germany; [4]Technische Universität München, ZIEL – Institute for Food & Health, Freising-Weihenstephan, Germany; [5]Division of Gastroenterology and Hepatology, Department of Internal Medicine, Medical University of Graz, Graz, Austria; [6]Technische Universität München, Chair of Proteomics and Bioanalytics, Freising-Weihenstephan, Germany; [7]Technische Universität München, Bavarian Center for Biomolecular Mass Spectrometry (BayBioMS), Freising-Weihenstephan, Germany; [8]OmicScouts GmbH, Freising, Germany; [9]RWTH University Hospital, Institute of Medical Microbiology, Functional Microbiome Research Group, Aachen, Germany; and [10]Vall d'Hebron Research Institute, Digestive Research Unit, Barcelona, Spain

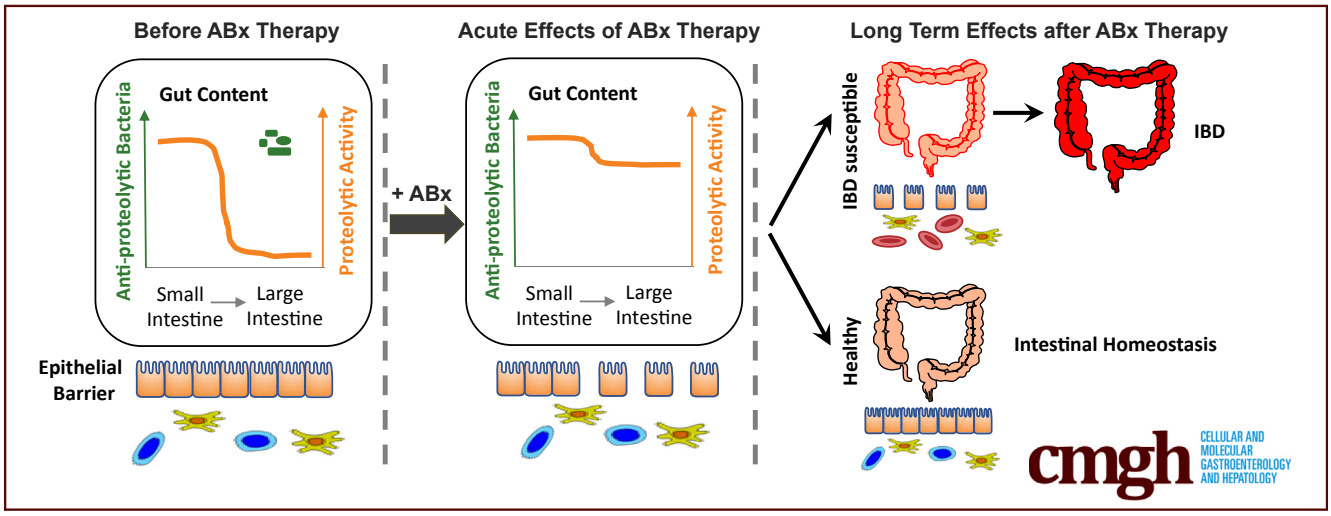

SUMMARY

Antibiotic therapies eliminate antiproteolytic bacteria in the large intestine, resulting in an increase in proteolytic activity, which is detrimental to the epithelial barrier function. In inflammatory bowel disease–susceptible individuals, high proteolytic activity promotes colitis development in the long term.

BACKGROUND & AIMS: Antibiotic (ABx) therapy is associated with increased risk for Crohn's disease but underlying mechanisms are unknown. We observed high fecal serine protease activity (PA) to be a frequent side effect of ABx therapy. The aim of the present study was to unravel whether this rise in large intestinal PA may promote colitis development via detrimental effects on the large intestinal barrier.

METHODS: Transwell experiments were used to assess the impact of high PA in ABx-treated patients or vancomycin/metronidazole-treated mice on the epithelial barrier. Serine protease profiling was performed using liquid chromatography–mass spectrometry/mass spectrometry analysis. The impact of high large intestinal PA on the intestinal barrier in wild-type and interleukin (IL)$10^{-/-}$ mice and on colitis development in $IL10^{-/-}$ mice was investigated using vancomycin/metronidazole with or without oral serine protease inhibitor (AEBSF) treatment.

RESULTS: The ABx-induced, high large intestinal PA was caused by significantly increased levels of pancreatic proteases and impaired epithelial barrier integrity. In wild-type mice, the rise in PA caused a transient increase in intestinal permeability but did not affect susceptibility to chemically induced acute colitis. In $IL10^{-/-}$ mice, increased PA caused a consistent impairment of the intestinal barrier associated with inflammatory activation in the large intestinal tissue. In the long term, the vancomycin/metronidazole-induced lasting increase in PA aggravated colitis development in $IL10^{-/-}$ mice.

CONCLUSIONS: High large intestinal PA is a frequent adverse effect of ABx therapy, which is detrimental to the large intestinal barrier and may contribute to the development of chronic intestinal inflammation in susceptible individuals. *(Cell Mol Gastroenterol Hepatol 2018;6:370–388; https://doi.org/10.1016/j.jcmgh.2018.05.008)*

Keywords: Epithelial Barrier; Serine Proteases; Gut Microbiota; Inflammatory Bowel Diseases.

See editorial on page 347.

Inflammatory bowel diseases (IBD), including Crohn's disease and ulcerative colitis, are idiopathic diseases that are thought to be the consequence of a dysregulated intestinal immune response toward the intestinal microbiota.[1-3] IBD are characterized by chronic inflammation, impaired intestinal barrier function, and microbial dysbiosis.[4-7] The highly complex etiology of IBD, comprising approximately 200 susceptibility loci[8] and abundant environmental factors,[9] results in an individual-specific pathogenesis from unknown initial triggers to the manifestation of the chronic inflammation. Interestingly, recent studies suggest a critical role of the microbial ecosystem in the initiation and progression of IBD.[10-13]

The intestinal microbiota of healthy individuals consists of highly diverse communities of microbes performing important functions, such as the production of short-chain fatty acids, metabolism of bile acids,[14] pathogen exclusion,[15] modulation of the intestinal immune system,[16] and degradation of pancreatic proteases in the large intestine.[17] In consequence, antibiotic (Abx)- or infection-induced microbial dysbiosis may exert a significant impact on the onset and progression of chronic metabolic or chronic inflammatory diseases in susceptible organisms.[18-21] Perturbations of the intestinal microbial ecosystem by ABx therapies were found to be associated with functional intestinal disorders, such as irritable bowel syndrome,[22,23] colorectal cancer,[24,25] overweight, and asthma.[26] In the context of IBD, several clinical studies have already revealed that early and frequent ABx therapies, especially metronidazole or fluoroquinolone treatments, are associated with increased risk for Crohn's disease.[27,28] However, the causal role of ABx therapies in the disease development and the mechanisms underlying this potential serious long-term adverse effect of ABx on the intestinal immune homeostasis remain unknown.

Interestingly, it has long been known that ABx treatments can result in increased luminal serine protease activity (PA) in the large intestine of rodents[29,30] or patients.[31,32] This increase in PA is assumed to be caused by the ABx-mediated eradication of yet unknown intestinal bacteria that normally inactivate the high load of pancreatic proteases on entry of the chyme into the large intestine.[33,34] The finding that *ex vivo* exposure of murine colonic mucosa to high PA fecal supernatants from patients with diarrhea-predominant irritable bowel syndrome can induce a serine protease-dependent increase of the mucosal permeability[35] indicates that the ABx-mediated rise in PA may be rather detrimental to the large intestinal barrier. In the context of IBD, reduced intestinal barrier functions and increased translocation of luminal antigens into the mucosal tissue are known to promote chronic inflammation.[36-39] In view of these data, we hypothesized that the ABx-increased PA in the large intestine is a relevant risk factor for the development of colitis in susceptible organisms.

Methods

Ethics Statement

The breeding and experimental use of mice in the animal facilities of the Technische Universität München (School of Life Sciences Weihenstephan) was approved by the local institution in charge (Regierung von Oberbayern; approval number 55.2-1-54-2531-99-13 and 55.2-1-54-2532-17-2015).

Stool Sample Collection From Patients

Samples were collected before and after ABx therapy at the Capio Hospital General de Catalunya in Barcelona[40] and the Medical University of Graz (ethical approval number 17-199 ex 05/06) and stored at -20°C until analysis. Patient characteristics are summarized in Table 1.

Experimental Design (Wild-Type and Interleukin $10^{-/-}$ Mice)

In all experiments, mice were fed with vancomycin/metronidazole (V/M)-containing chow mash or control (ctr) mash *ad libitum* for the indicated period of time. V/M mash (Fluka, Seelze, Germany) was prepared by mixing a vancomycin (0.25 g/L; Fluka)/metronidazole (1.0 g/L; Sigma-Aldrich, Steinheim, Germany) solution with chow powder (ssniff-Spezialdiäten GmbH, Soest, Germany) in a 1:1 volume (mL)/weight (g) ratio.

In the short-term experiments, 8-week-old wild-type (WT) (C57BL/6, male and female) or interleukin (IL) $10^{-/-}$ mice (129/SvEv, male and female) (n $\geq$5/group) were treated with V/M for either 2 days, 7 days, or left untreated. The protease inhibitor 4-(2-aminoethyl) benzenesulfonyl fluoride hydrochloride (300 mg/kg body weight) (AEBSF; Sigma-Aldrich) or water was applied by oral gavage starting from 1 day before V/M treatment where indicated. Fresh fecal pellets were sampled daily from all mice. Fluorescein

***Authors share co-correspondence authorship.**

Abbreviations used in this paper: **ABx, antibiotics; AEBSF, 4-(2-aminoethyl) benzenesulfonyl fluoride hydrochloride; cecal-sup, cecal-supernatants; ctr, control; DSS, dextran sulfate sodium; GF, germ-free; IBD, inflammatory bowel diseases; IL, interleukin; LC-MS/MS, liquid chromatography–mass spectrometry/mass spectrometry; PA, protease activity; PBS, phosphate-buffered saline; PMSF, phenylmethane-sulfonylfluoride; stool-sup, stool-supernatants; SPF, specific pathogen-free; TEER, transepithelial electrical resistance; V/M, vancomycin/metronidazole; WT, wild-type.**

Most current article

2352-345X
https://doi.org/10.1016/j.jcmgh.2018.05.008

Table 1. Patient Characteristics

Classification	ABx name	ABx therapy duration, *d*	Indication	Fold increase in PA	Diarrhea (after ABx)
Fluoroquinolone (+Imidazole)	Levofloxacin	7	Bronchitis	7.57	No
	Levofloxacin	7	Bronchitis	0.30	No
	Levofloxacin	7	Bronchitis	3.04	No
	Levofloxacin	7	Bronchitis	2.35	No
	Levofloxacin	7	Bronchitis	5.50	No
	Levofloxacin	7	Bronchitis	1.83	No
	Ciprofloxacin	7	UC	13.59	No
	Levofloxacin	7	Bronchitis	0.32	No
	Levofloxacin+metronidazole	7	*Clostridium difficile* infection	8.27	No
β-Lactam	Amoxicillin+clavulanate	7	Bacteremia	12.74	No
	Amoxicillin+clavulanate	7	Bronchitis	0.96	No
	Amoxicillin+clavulanate	7	Bacteremia	1.43	No
	Amoxicillin+clavulanate	7	Bronchitis	1.02	No
	Amoxicillin+clavulanate	7	Urinary infection	2.23	No
	Amoxicillin+clavulanate	7	Bronchitis	0.26	No
	Amoxicillin+clavulanate	7	Bronchitis	0.37	No
Cephalosporin (+macrolide)	Azithromycin	2	CD	6.10	No
	Ceftriaxone+azithromycin	7	Pneumonia	0.41	No
	Ceftriaxone+azithromycin	7	Bronchitis	1.29	No
	Ceftriaxone	7	Urinary infection	0.51	No
Rifamycin	Rifaximin	3	IBS	10.49	No
	Rifaximin	3	IBS	0.34	No
	Rifaximin	3	IBS	0.45	No
	Rifaximin	3	IBS	2.49	No
	Rifaximin	3	IBS	2.17	No
	Rifaximin	3	IBS	0.82	Yes
	Rifaximin	3	IBS	0.77	No
	Rifaximin	3	IBS	1.85	No
	Rifaximin	3	IBS	0.92	Yes
	Rifaximin	3	IBS	0.73	Yes
	Rifaximin	3	IBS	0.64	Yes
	Rifaximin	3	IBS	5.36	No

ABx, antibiotic; CD, Crohn's disease; IBS, inflammatory bowel syndrome; PA, protease activity; UC, ulcerative colitis.

isothiocyanate dextran (4 kDa; Sigma-Aldrich) was applied by oral gavage 4 hours before mice were sacrificed by CO_2.

In the long-term experiments, WT (male) and IL10$^{-/-}$ mice (male and female) (n $\geq$5/group) were treated with V/M for 7 days at the age of 4 and 8 weeks or left untreated. Fresh fecal pellets were sampled on a weekly basis. At 12 weeks of age, WT mice were exposed to 1.5% dextran sulfate sodium (DSS; Sigma-Aldrich) in drinking water for 7 days and sacrificed at Day 9. The severity of DSS-induced colitis was monitored by daily determination of the disease activity index. From IL10$^{-/-}$ mice, facial blood was collected every second week from the age of 10–16 weeks. IL10$^{-/-}$ mice were sacrificed at 16 weeks of age.

Colonization of Germfree Mice

Cecal microbiota from untreated or V/M-treated specific pathogen-free (SPF) mice was prepared as described[12] and orally administered to germ-free (GF) mice (10 weeks of age). Mice were sacrificed 2 weeks after the transfer.

Preparation of Cecal Content/ Stool-Supernatants

Cecal content/stool-supernatants (cecal-sup/stool-sup, 10% wt/vol) were generated from the cecal contents of WT, IL10$^{-/-}$ mice, or patient stool. A total of 100 mg of patient stool or murine gut contents from the ileum, cecum, colon, or feces were homogenized and dissolved in sterile phosphate-buffered saline (PBS, 10% wt/vol) using sterile glass beads and vigorous vortexing. Supernatant was generated by a 2-step centrifugation (5 min, 1000 rpm, 4°C) followed by centrifugation of the resulting supernatant (10 min, 6000 rpm, 4°C). Whenever indicated, the supernatants were incubated with the serine protease inhibitor phenylmethane-sulfonylfluoride (PMSF; 5 mM; Sigma-Aldrich). The supernatants were stored at -20°C.

Table 2. Disease Activity Score

Score	Weight loss (%)	Stool consistency	Blood in stool
0	0	Normal	No blood
1	Lower than 5	—	—
2	Lower than 10	Slightly changed	Positive
3	Lower than 15	—	Positive for 2 d
4	Lower than 20	Diarrhea	Positive for more than 2 d

Table 3. Primer Sequences and UPL Probe IDs for Quantitative Polymerase Chain Reaction Analysis

Gene	Forward primer	Reverse primer	Probe
IFNγ	5'-cctttggaccctctgacttg	5'-agcgttcattgtctcagagcta	63
IL-1β	5'-tgtaatgaaagacggcacacc	5'-tcttctttgggtattgcttgg	78
C3	5'-accttacctcggcaagtttct	5'-ttgtagagctgctggtcagg	76
CD3	5'-cttgtacctgaaagctcgagtg	5'-gatgattatggctactgctgtca	10
GAPDH	5'-tccactcatggcaaattcaa	5'-tttgatgttagtggggtctcg	9

Protease Activity Assay

The tryptic activity in gut content supernatants was analyzed using the Protease Assay Kit (Calbiochem, EMD Millipore Corp, Billerica, MA) according to the manufacturerś instructions. In short, 10 μL of the respective supernatant were incubated with FTC-casein solution (1 hour, 37°C). Fluorescence was subsequently measured using an Infinite 200 PRO plate reader (Tecan Group Ltd, Männedorf, Switzerland).

Visualization of Active Serine Proteases

Gut content supernatants were incubated with ActivX TAMRA-FP Probes (1 μM; Thermo Fisher Scientific, Rockford, IL) (30 min, RT, in the dark). The mixture was diluted with 2X sodium dodecyl sulfate buffer, boiled (5 min, 95°C), and subjected to gel electrophoresis on 15% sodium dodecyl sulfate–polyacrylamide gel electrophoresis. Labelled proteins were detected using a Typhoon Trio+ scanner (GE Health Care Science, Buckinghamshire, UK).

Ex Vivo *Incubation Assay*

Fresh cecal bacteria (1 × 109) isolated from SPF- or V/M-treated mice were incubated with cecal-sup (50 μL) from GF mice for 24 hours at 37°C. To heat-inactivate bacteria, bacteria were boiled for 20 minutes at 95°C before incubation with cecal-sup. After the incubation for 24 hours, 10 μL of the supernatants were used for the PA assay.

Liquid Chromatography–Mass Spectrometry/Mass Spectrometry Analysis

Proteome analysis of cecal-sup from ctr, V/M-treated, and GF mice was performed using liquid chromatography–mass spectrometry/mass spectrometry (LC-MS/MS) analysis. Cecal-sup was diluted 1:1 with 2×NuPAGE LDS Sample Buffer (Invitrogen, Darmstadt, Germany) and proteins were reduced by 10 mM dithiothreitol and alkylated by 55 mM iodoacetamide. Samples were then run into a 4%–12% NuPAGE gel (Invitrogen) for about 1 cm to concentrate the

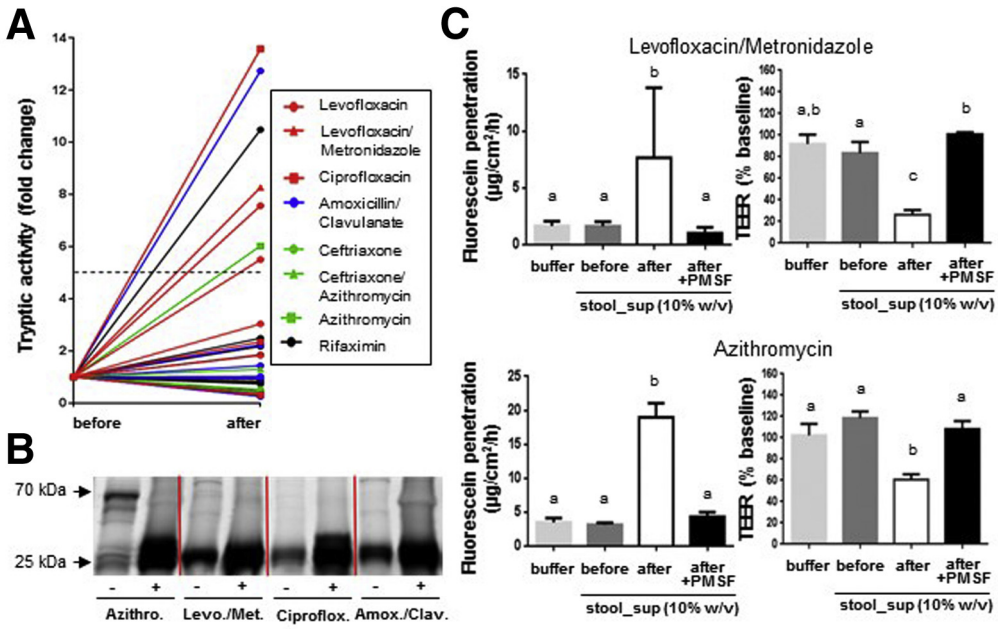

Figure 1. High stool PA is a frequent adverse effect of ABx treatment in patients and impairs the epithelial barrier *ex vivo*. (*A*) Serine protease activity in stool-supernatant of patients before and after ABx treatment. *Red line* (n = 9), fluoroquinolone (+imidazole) antibiotic; *blue line* (n = 7), β-lactam antibiotic; *green line* (n = 4), cephalosporin (+macrolide) antibiotic; *black line* (n = 12), rifamycine antibiotic. (*B*) Staining of active serine proteases in stool-supernatants of patients before and after ABx treatment (TAMRA-FP sodium dodecyl sulfate–polyacrylamide gel electrophoresis). (*C*) Fluorescein translocation and TEER in polarized PTK6 cells on apical exposure to stool-supernatants from the same patient before versus after the respective ABx treatment ± PMSF-inhibition.

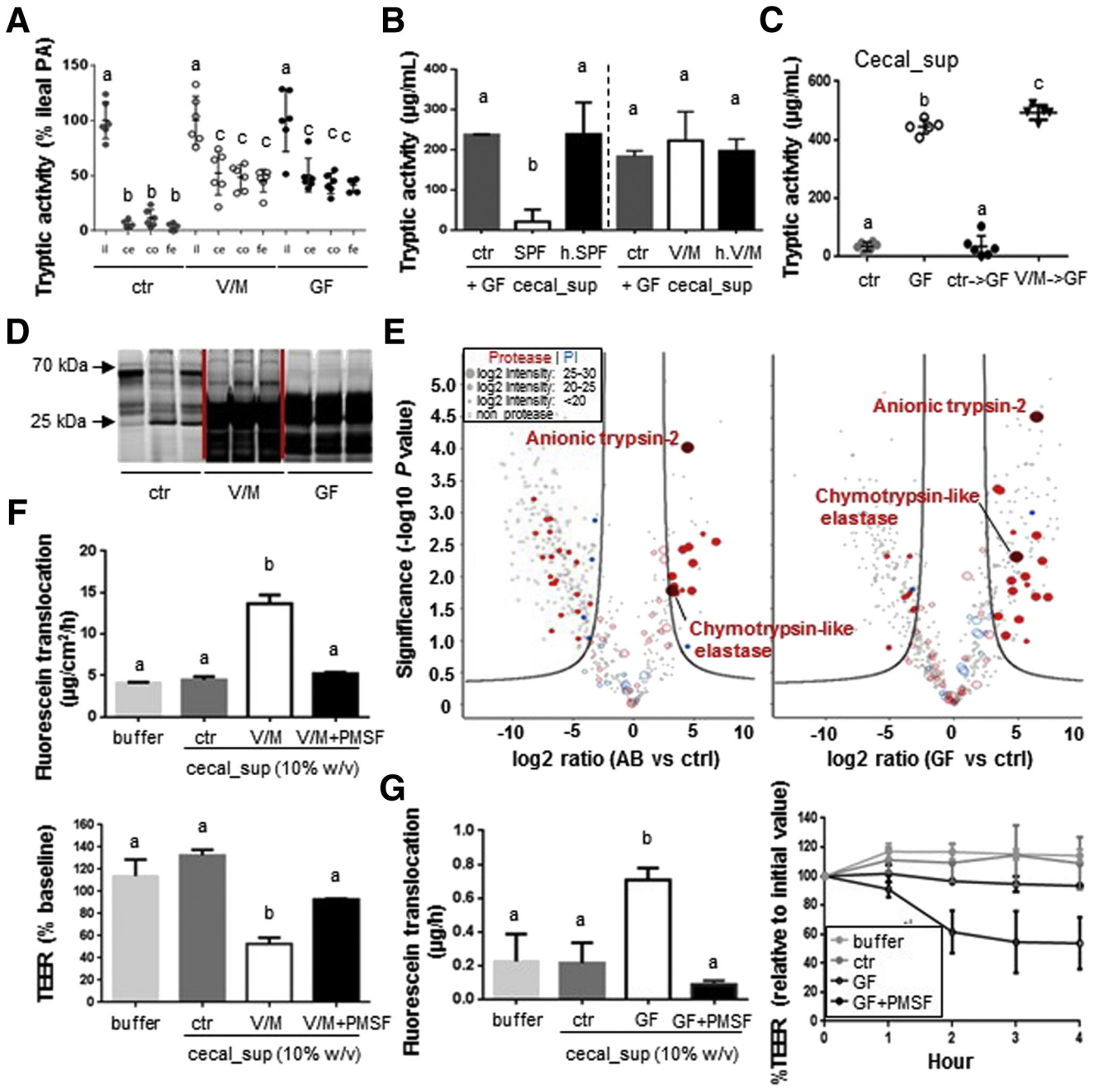

Figure 2. Eradication of antiproteolytic bacteria by V/M treatment results in excessive large intestinal PA and impairs the epithelial barrier *ex vivo*. (*A*) Comparison of the level of luminal serine protease activity in the ileum (il), cecum (ce), colon (co), and feces (fe) of untreated SPF (ctr), V/M-treated (V/M), and GF mice. (*B*) Bacteria were isolated from fresh cecum content of SPF or V/M-treated mice, and cecal-sup from GF mice was incubated for 24 hours with buffer (ctr), the respective freshly isolated bacteria, or heat-killed (h.) bacteria. The remaining serine protease activity in GF cecal-sup was measured after the incubation. (*C*) Protease activity in cecal-sup of ctr mice, GF mice, GF mice associated with cecal microbiota from either ctr SPF mice (ctr->GF), or V/M-treated SPF mice for 2 weeks (V/M->GF). (*D*) Staining of active serine proteases in cecal-sup of ctr, V/M, or GF mice (TAMRA-FP sodium dodecyl sulfate–polyacrylamide gel electrophoresis). (*E*) Volcano plot showing all murine proteases (*red*) and protease inhibitors (PI, *blue*) that were detected via LC-MS/MS analysis in cecal-supernatants of ctr, V/M, or GF mice (n = 3/group). The log2 intensity (depicted by the dot size) indicates the abundance of the respective protein. The proteins on the right side of the volcano blots are significantly higher abundant in V/M-treated or GF mice, respectively, compared with control mice. (*F*) Fluorescein translocation and TEER in polarized PTK6 cells on apical exposure to cecal-sup from ctr mice versus V/M-treated mice ± PMSF inhibition. (*G*) Colonic tissue sections from SPF mice were apically exposed to cecal-sup from control SPF (ctr) mice or cecal-sup from GF mice ± PMSF in an Ussing chamber setup. Translocation of apically applied fluorescein to the basolateral side and TEER of the respective tissue sections were measured.

sample before in-gel tryptic digestion. In-gel trypsin digestion was performed according to standard procedures.[41]

Peptides generated by in-gel trypsin digestion were dried in a vacuum concentrator and then dissolved in 20 μL 0.1% formic acid before LC–MS/MS analysis. LC–nanoESI-MS/MS was performed by coupling a nanoLC-Ultra (Eksigent Technologies, Dublin, CA) to an LTQ-Orbitrap Velos mass spectrometer (Thermo Fisher Scientific,

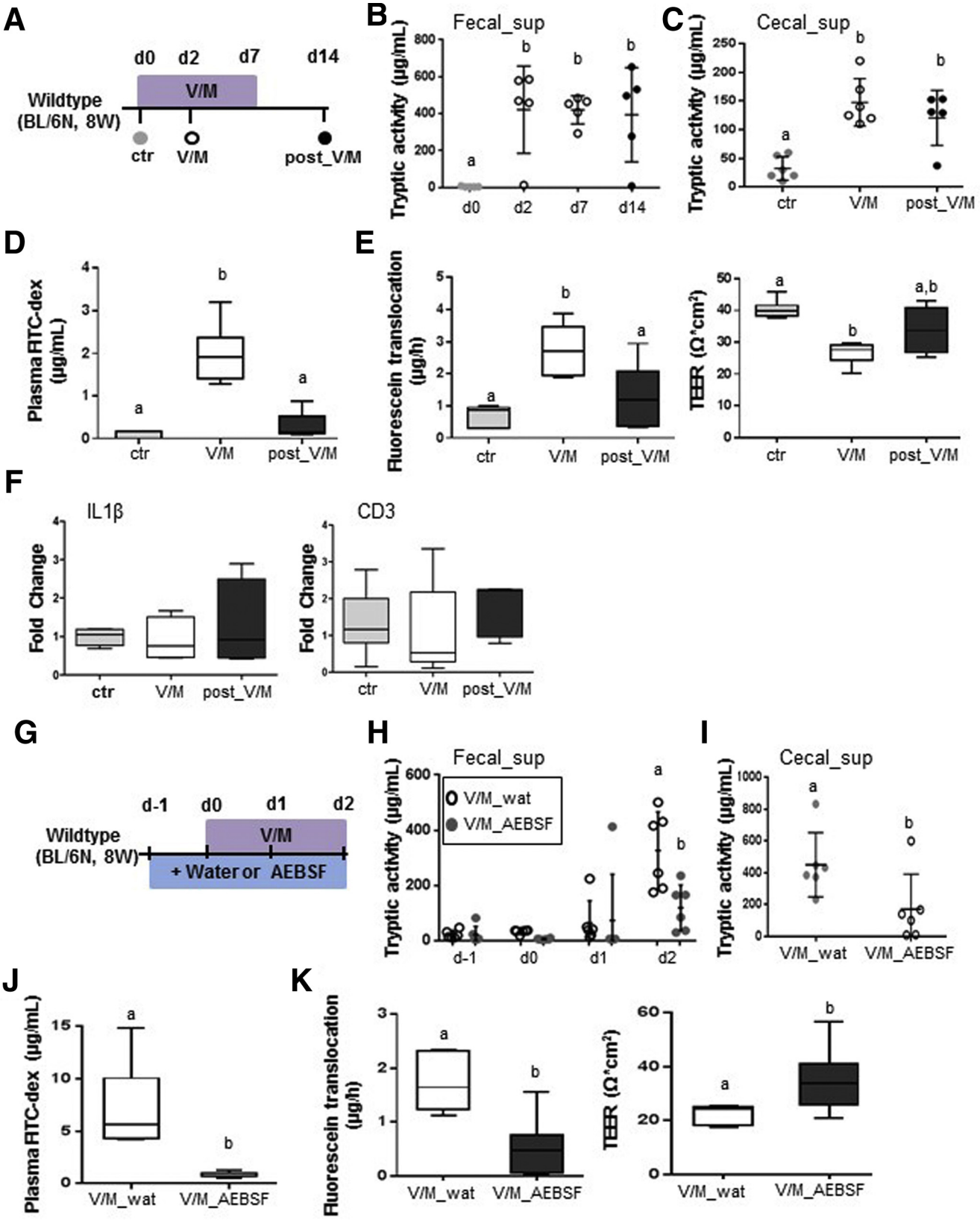

Schwerte, Germany). For each analysis, 10 μL of dissolved peptides was delivered to a trap column (ReproSil-pur C18-AQ, 5 μm, Dr. Maisch, Ammerbuch, Germany, 20 mm $\times$ 75 μm, self-packed) at a flow rate of 5 μL/min in 100% solvent A (0.1% formic acid in high-performance liquid chromatography grade water). After 10 minutes of loading and washing, peptides were transferred to an analytical column (ReproSil-gold C18-AQ, 3 μm, Dr. Maisch, Ammerbuch, Germany, 400 mm $\times$ 75 μm, self-packed) and separated using a 210-minute gradient from 2% to 32% of solvent B (0.1% formic acid in acetonitrile) at 300 nL/min flow rate. Both LC solvents contained 5% (vol/vol) dimethyl sulfoxide to boost the nanoESI response of peptides.[42] The LTQ Orbitrap Velos was operated in data-dependent mode, automatically switching between MS and MS/MS. Full-scan MS spectra (360–1300 m/z) were acquired in the Orbitrap at 30,000 resolution (at m/z 400) after accumulation of precursor ions to a target value of 1,000,000 for a maximum time of 100 ms. Internal lock mass calibration was performed using an ion signal (m/z 401.922720) present in dimethyl sulfoxide containing solvents.[42] Tandem mass spectra were generated for up to 10 peptide precursors by higher energy collision-induced dissociation (target value of 40,000, max 100 ms accumulation time, isolation width 2.0 Th) at a normalized collision energy of 30% and fragment ions were recorded at a resolution of 7500 in the Orbitrap. To maximize the number of precursors targeted for analysis, dynamic exclusion was enabled with 1 repeat count in 10-second and 20-second exclusion time (mass tolerance $\pm$ 10 ppm).

Label-free quantification was performed using MaxQuant (version 1.5.3.30)[43] by searching MS data against a mus musculus UniProt reference database (version 03.05.2016, 24864 entries) using the search engine Andromeda.[44] Carbamidomethylated cysteine was used as fixed modification; variable modifications included oxidation of methionine and N-terminal protein acetylation. Trypsin/P was specified as proteolytic enzyme with up to 2 allowed miscleavage sites. Precursor tolerance was set to 4.5 ppm and fragment ion tolerance was set to 20 ppm. Label-free quantification,[45] match-between-runs, and intensity-based absolute quantification options were enabled and results were filtered for a minimal length of 7 amino acids, 1% peptide, and protein FDR and reverse identifications.

MaxQuant results were imported into the MaxQuant associated software suite Perseus (v.1.5.6.0).[46] iBAQ intensities were filtered for at least 2 valid values per experimental group and at least 2 peptides for identification per protein. Missing values were imputed from normal distribution (width 0.3, downshift 1.8). A 2-sided Student *t* test was performed to assess statistical significance. Protein *P* values were corrected for multiple testing using a permutation based 5 % FDR cutoff (250 randomizations, s0 of 3.37).

The mass spectrometry proteomics data have been deposited to the ProteomeXchange Consortium (http://proteomecentral.proteomexchange.org) via the PRIDE partner repository with the dataset identifier PXD007914.

Colonic Epithelial Cell (PTK6 cell) Culture, Transepithelial Electrical Resistance Measurement, and Permeability Assay

PTK6 cells (colonic epithelial cells, 1.5 $\times$ 10^5 cells/well) were seeded on Transwells (polyester membrane with pore size of 0.4 μm, Corning Inc, Kennebunk, ME) and cultured with RPMI-1640 medium including insulin transferrin selenium A and fetal calf serum (5% CO_2, 37°C) until the transepithelial electrical resistance (TEER) reached a value >1.0 kΩ. PTK6 cells were then stimulated with cecal-sup/stool-sup (10% wt/vol), which was prepared in RPMI-1640 medium without fetal calf serum on the apical side (fresh medium without fetal calf serum on basolateral side). TEER was measured on a heating block (Thermo Fisher Scientific) to maintain a constant temperature at 37°C. After the TEER measurements, the medium on the basolateral side was replaced by fresh Krebs buffer and the one on the apical side was replaced by fresh Krebs buffer supplemented with fluorescein (500 μg/mL). The PTK6 cells were subsequently incubated for 30 minutes at 37°C. The level of translocation of fluorescein through the epithelial layer was determined via the measurement of fluorescence in the Krebs buffer on the basolateral side (emission at 538 nm).

Ussing Chamber Analysis

The permeability and TEER of cecal/colonic tissue from V/M-treated/untreated WT or IL10$^{-/-}$ mice were measured by Ussing chamber analysis. Segments of the cecum and the distal colon (1 cm each) were cut open, gut contents were carefully removed, and the tissue was mounted in the Ussing chamber. The mounted tissues were connected to a voltage clamp apparatus and incubated in Krebs buffer (95% O_2, 5% CO_2, 37°C). The tissues were equilibrated for 20 minutes and TEER was measured (for 2 hours, every 30 minutes) by Acquire & Analyze 2.3 software. To assess the intestinal permeability, fluorescein (50 mg/mL) was loaded to the apical side after the TEER measurement. The Krebs buffer on the basolateral side was collected and the level of fluorescence was determined (emission at 538 nm).

To investigate the impact of high PA on large intestinal tissue from ctr SPF mice *ex vivo*, the mucosal side of the tissue sections was exposed to cecal-sup (10% wt/vol) from

Figure 3. (***See previous page***). **Excessive large intestinal PA results in transient impairment of the intestinal barrier in WT mice.** (*A*) Experimental schedule: untreated WT mice (ctr), V/M-treated WT mice at Day 2 of the treatment (V/M), and V/M-treated WT mice 7 days after discontinuation of the treatment (post-V/M) were investigated. (*B*, *C*) Fecal and cecal serine protease activity. (*D*) Plasma concentration of fluorescein isothiocyanate (FITC) dextran 4 hours after oral gavage of FITC dextran (4 kDa). (*E*) Ussing chamber analyses of fluorescein translocation and TEER in cecal tissue sections. (*F*) mRNA expression levels of IL1β and CD3 in colonic tissue. (*G*) Experimental schedule: V/M-treated WT mice were cotreated (oral gavage) with the serine protease inhibitor AEBSF (V/M AEBSF) or H_2O (V/M wat), starting from 1 day before V/M treatment. (*H*, *I*) Fecal and cecal serine protease activity. (*J*) Plasma concentration of FITC dextran 4 hours after oral gavage of FITC dextran (4 kDa). (*K*) Ussing chamber analyses of fluorescein translocation and TEER in cecal tissue sections.

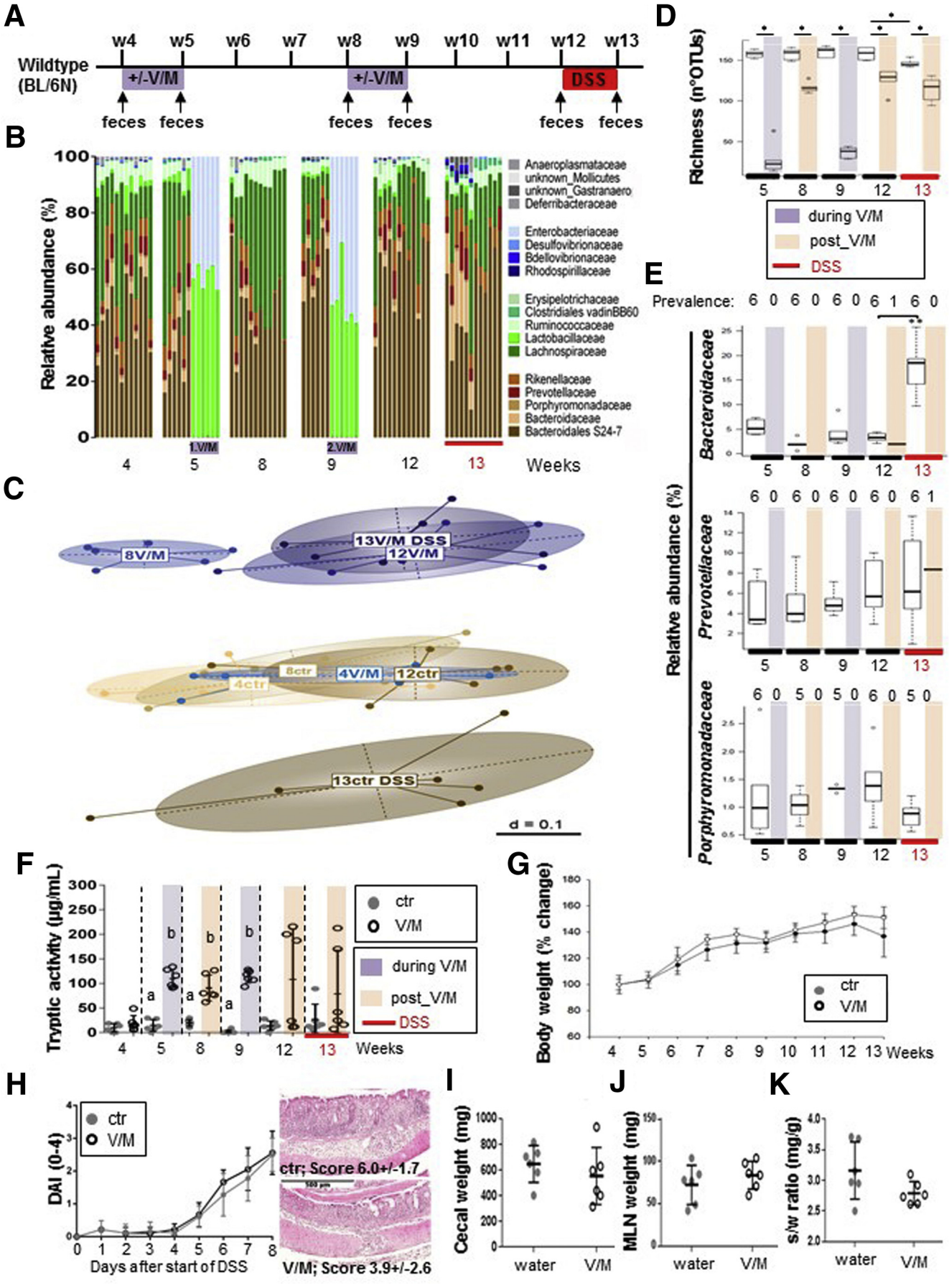
A
w4 w5 w6 w7 w8 w9 w10 w11 w12 w13
Wildtype (BL/6N)
+/-V/M
+/-V/M
DSS
feces feces feces feces feces feces
B
Relative abundance (%)
Anaeroplasmataceae
unknown_Mollicutes
unknown_Gastranaero
Deferribacteraceae
Enterobacteriaceae
Desulfovibrionaceae
Bdellovibrionaceae
Rhodospirillaceae
Erysipelotrichaceae
Clostridiales vadinBB60
Ruminococcaceae
Lactobacillaceae
Lachnospiraceae
Rikenellaceae
Prevotellaceae
Porphyromonadaceae
Bacteroidaceae
Bacteroidales S24-7
1.V/M
2.V/M
Weeks
C
8V/M
13V/M DSS
12V/M
8ctr
4V/M
12ctr
4ctr
13ctr DSS
d = 0.1
D
Richness (n°OTUs)
during V/M
post_V/M
DSS
E
Prevalence:
Relative abundance (%)
Bacteroidaceae
Prevotellaceae
Porphyromonadaceae
F
Tryptic activity (µg/mL)
ctr
V/M
during V/M
post_V/M
DSS
Weeks
G
Body weight (% change)
ctr
V/M
Weeks
H
DAI (0-4)
ctr
V/M
Days after start of DSS
ctr; Score 6.0+/-1.7
V/M; Score 3.9+/-2.6
I
Cecal weight (mg)
water
V/M
J
MLN weight (mg)
water
V/M
K
s/w ratio (mg/g)
water
V/M

SPF or GF mice ± PMSF (5 mM) for 4 hours and TEER was measured every hour. To assess the impact of the respective cecal-sup on the permeability, fluorescein was added to the apical chamber for 30 minutes after the last TEER measurement and the level of basolateral fluorescein was measured as described previously.

Tissue Processing, Hematoxylin-Eosin, and Immunofluorescence Staining

Cecal and colonic tissue was fixed in formaldehyde (4%) and embedded in paraffin. For hematoxylin-eosin staining, the severed sections (4 μm) were stained with hematoxylin-eosin (0.2%) before mounting. The stained sections were visualized by Zeiss Axioskop 40 microscope (Zeiss).

For the immunofluorescence staining of $CD3^+$ T cells, antigen unmasking was performed by boiling tissue sections (4 μm) in 10 mM citrate buffer (pH 6, 900 W, 23 minutes) in a pressure cooker. Then, the sections were incubated in blocking buffer including 5% rabbit serum for 1 hour at RT after a rinse with PBS. The sections were incubated overnight with the primary antibody (CD3, 1:200, Sigma-Aldrich) at 4°C and then rinsed with PBS. The sections were incubated with fluorescence-conjugated secondary antibodies (antirabbit AF594, 1:200, Life Technologies, Carlsbad, CA) for 1 hour at RT. All sections were counterstained with DAPI (1:2000, Sigma-Aldrich) and fluorescence measurements were performed using Flouview FV10i microscope (Olympus, Shinjuku, Japan).

Histopathology

Histopathologic inflammation was blindly assessed by an independent pathologist using an established scoring system (score from 0 to 12).[47,48] Images were acquired by Touch microscope V. precipoint (PreciPoint GmbH, Freising, Germany).

Disease Activity Index

The disease activity index in DSS-treated mice was determined by daily monitoring of weight loss, stool consistency, and occult blood (scores range from 0 to 4 as described in Table 2). The disease activity index is the average of these individual scores/mouse/day.

Quantitative Real-Time Polymerase Chain Reaction

RNA from cecal and colonic tissue was extracted with RA1 buffer (Macherey-Nagel, Düren, Germany) using NucleoSpin RNAII kit (Macherey-Nagel GmbH). cDNA was synthesized using 500 ng total RNA, random hexamers, and MMLV reverse transcriptase Point Mutant Synthesis System (Promega, Fitchburg, WI). For the real-time polymerase chain reaction, the amplification was performed with Universal Probe Library system in a Light Cycler 480 system (Roche Diagnostics, Mannheim, Germany). The primers and probes are described in Table 3.

Serum Amyloid A and Complement C3 Enzyme-Linked Immunosorbent Assay

Plasma serum amyloid A and fecal complement C3 levels were measured by enzyme-linked immunosorbent assay (Immunology Consultants Laboratory Inc, Portland, OR) according to the manufacturer instructions.

16S Ribosomal RNA Gene Amplicon Analysis

Metagenomic DNA from the cecal contents of repeatedly V/M-treated WT and $IL10^{-/-}$ mice was isolated using a modified protocol according to Godon et al.[49] Briefly, snap-frozen samples were thawed on ice, mixed with 600 μL stool DNA stabilizer (Stratec, Beringen, Switzerland), and transferred into autoclaved 2-mL screw-cap tubes containing 500-mg, 0.1-mm diameter silica/zirconia beads. After addition of 250 μL 4 M guanidine thiocyanate in 0.1 M Tris (pH 7.5) and 500 μL 5 % N-lauroyl sarcosine in 0.1 M PBS (pH 8.0), samples were incubated at 70°C and 700 rpm for 60 minutes. A FastPrep instrument (MP Biomedicals, Santa Ana, CA) fitted with a 24 × 2 mL cooling adaptor filled with dry ice was used for cell disruption. The program was run 3 times for 40 seconds at 6.5 M/s. After each run, the cooling adapter was refilled with dry ice. An amount of 15 mg polyvinylpyrrolidone was added and samples were vortexed, followed by 30-minute centrifugation at 15.000 × g and 4°C. Approximately 650 μL of the supernatant were transferred into a new 2-mL tube, which was centrifuged again for 3 minutes at 15.000 × g and 4°C. Subsequently, 500 μL of the

Figure 4. (***See previous page***). **Excessive large intestinal PA does not disturb the intestinal immune homeostasis in WT mice.** (*A*) Long-term experimental setup: WT mice were left untreated (ctr) or repeatedly treated with V/M (2 times for 7 days at the age of 4 and 8 weeks) (V/M) before acute DSS colitis was induced at the age of 12 weeks (n = 6/group). (*B*) Overview on the V/M-mediated and DSS-mediated compositional dynamics in the intestinal microbiota of V/M-treated mice compared with ctr mice (family level). (*C*) Overview on the long-term impact of V/M treatment on the phylogenetic makeup (beta-diversity) of cecal microbiota and its response to DSS treatment. (*D*) Richness of the intestinal microbiota. (*E*) Relative abundance of *Bacteroidaceae*, *Prevotellaceae*, and *Porphyromonadaceae* in untreated versus V/M-treated WT mice before and after exposure to DSS. The number of mice in which the respective bacterial family was detected (prevalence) is depicted above the respective figure. Color code: *purple* = during V/M treatment, *light red* = post V/M treatment (after first and second V/M treatments), *red* = DSS treatment. (*F*) Kinetic of the fecal serine protease activity in untreated (ctr) versus V/M-treated (V/M) WT mice. (*G*) Body weight development in ctr and V/M-treated WT mice. (*H*) The *left panel* shows the development of the disease activity index after induction of acute colitis by DSS. The *right panel* shows representative hematoxylin-eosin stainings including the mean histopathological score of colonic tissue from DSS-treated ctr versus DSS-treated V/M-pretreated mice at Day 8 after the induction of DSS colitis. (*I–K*) Organ weight in DSS-treated ctr and V/M-pretreated WT mice. DAI, disease activity index.

supernatant was transferred into a new 2-mL tube and 50 μg of RNase was added. After 20 minutes at 37°C and 700 rpm, gDNA was isolated using the NucleoSpin gDNA Clean-up Kit from Macherey-Nagel according to the manufacturer protocol. DNA was eluted from columns twice using 40 μL Elution buffer and concentration was measured with NanoDrop (Thermo Fisher Scientific). Samples were stored at -20°C.

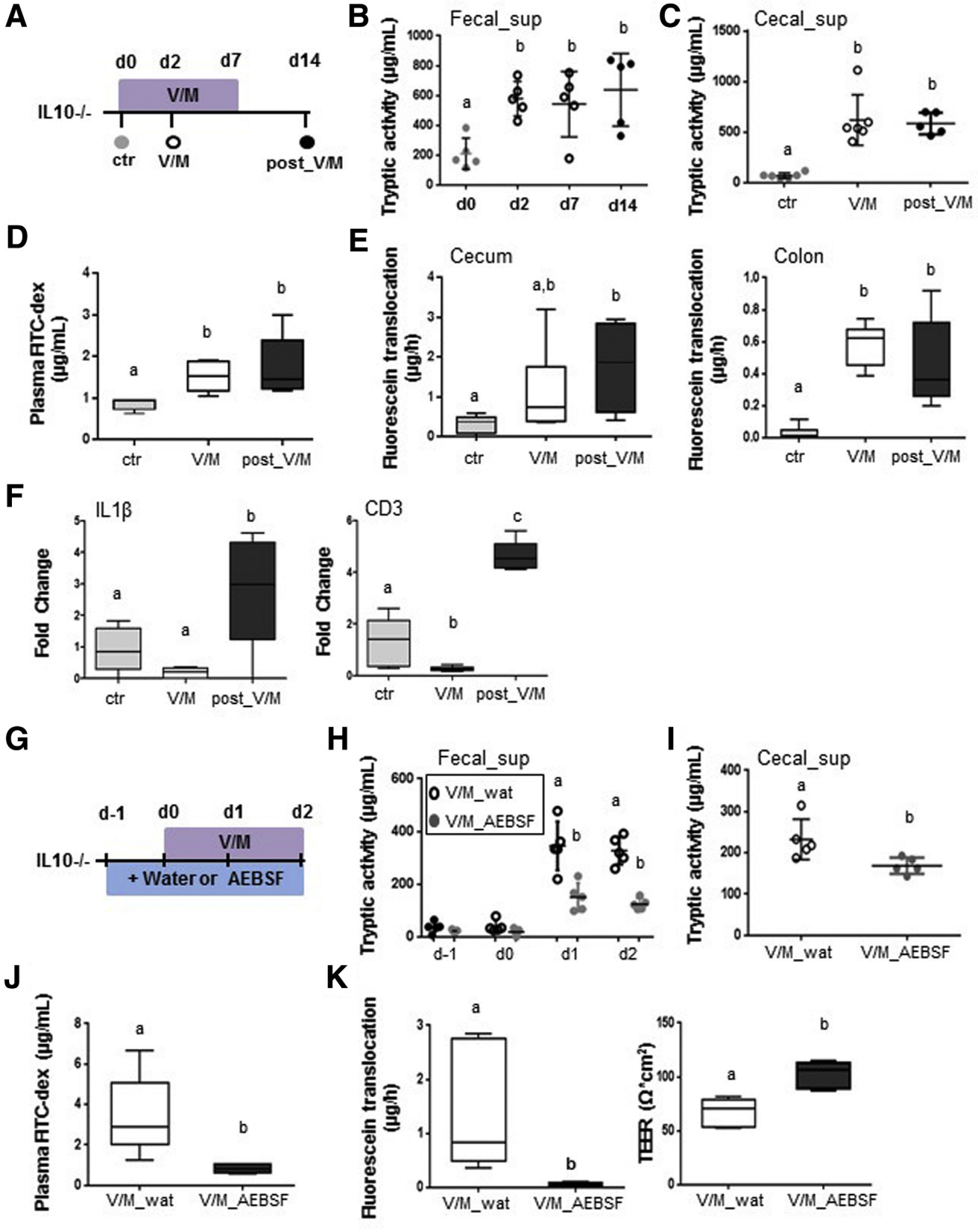

Library preparation and sequencing were performed as described in detail previously.[50] Samples were processed in a semiautomated manner using a Biomek-4000 robot (Beckman-Coulter, Brea, CA). Briefly, the V3-V4 region of 16S rRNA genes was amplified (25 cycles) following a 2-step protocol[51] using primers 341F-785R.[52] After purification using the AMPure XP system (Beckmann), sequencing was carried out with pooled samples in paired-end modus (PE275) using a MiSeq system (Illumina, San Diego, CA) according to the manufacturer instructions and 25% (vol/vol) PhiX standard library.

Data were analyzed as described in detail previously.[50] Raw reads were processed using an in-house developed pipeline (www.imngs.org)[53] based on UPARSE.[54] In brief, sequences were demultiplexed, trimmed to the first base with a quality score <3, and then paired. Sequences with less than 380 and more than 480 nucleotides and paired reads with an expected error >3 were excluded from the analysis. Remaining reads were trimmed by 10 nucleotides on each end to avoid GC bias and nonrandom base composition. The presence of chimeras was tested using UCHIME.[55] Operational taxonomic units were clustered at 97% sequence similarity, and only those with a relative abundance >0.5% in at least 1 sample were kept. Taxonomies were assigned at 80% confidence level using the RDP classifier.[56]

Downstream analysis was performed in the R programming environment using Rhea (https://lagkouvardos.github.io/Rhea/).[57] Operational taxonomic unit tables were normalized to account for differences in sequence depth. ß-diversity was computed based on generalized UniFrac distances.[58] α-diversity was assessed on the basis of species richness and Shannon effective diversity.[59] *P* values were calculated using analysis of variance on ranks and corrected for multiple comparisons according to the Benjamini-Hochberg method. Only taxa with a prevalence of at least 30% samples in one given group were considered for statistical analysis.

Statistics

Data are presented as mean ± SD. Statistical significance was determined by unpaired Student *t* test or analysis of variance with 1-way analysis of variance followed by Tukey posttest using Graph-Pad Prism (Graph Pad, version 6.01). $P < .05$ was considered as statistically significant.

Results

High Fecal Protease Activity in Antibiotic-Treated Patients Impairs the Epithelial Barrier

To assess the impact of frequently prescribed ABx therapies on the large intestinal PA, patient stool sampled before and after ABx treatments was analyzed, demonstrating a major (>5-fold) increase in PA in 25% of the investigated patients (Figure 1*A*, Table 1). Pattern analysis of active serine proteases revealed a major increase in low-molecular-weight proteases (<25 kDa) in the stool of these patients (Figure 1*B*), indicating high levels of pancreatic proteases, such as trypsin (~23.5 kDa) and chymotrypsin (~24.8 kDa) on ABx treatment. To assess the impact of the high stool PA on the epithelial barrier, polarized PTK6 cells were apically exposed to stool-sup from patients that showed a rise in fecal PA on ABx therapy. Whereas the epithelial barrier was not affected by exposure to the low PA present in stool-sup from patients before ABx therapy, the high PA in stool-sup from the same patient after ABx treatment significantly increased epithelial permeability and reduced TEER. The detrimental effect of high PA stool-sup from ABx-treated patients on the epithelial barrier was abrogated by prior serine protease inhibition via PMSF (Figure 1*C*). Of note, apical exposure to PMSF alone did not alter epithelial barrier functions (data not shown).

Eradication of Antiproteolytic Bacteria by Vancomycin/Metronidazole Treatment Results in Excessive Large Intestinal Protease Activity and Impairs the Epithelial Barrier Ex Vivo

To investigate the physiological relevance of ABx-increased PA, oral application of V/M was used in different experimental setups. V/M treatment of colonized mice resulted in large intestinal PA levels comparable with GF mice (Figure 2*A*), indicating highly efficient eradication of antiproteolytic bacteria by this ABx treatment. The V/M-mediated loss of anti-PA in the large intestinal microbiota was confirmed via an *ex vivo* incubation assay (Figure 2*B*) and gnotobiotic studies (Figure 2*C*). In the latter case, GF mice exposed to cecal microbiota from SPF mice showed normalized low PA levels 2 weeks after colonization, whereas cecal microbiota from V/M-treated mice was not able to mediate this effect.

Analogous to the observation in stool from ABx-treated patients, cecal content from V/M-treated mice showed a strong increase in active, low-molecular-weight serine proteases (<25 kDa) (Figure 2*D*). LC-MS/MS analysis of cecal-sup revealed significantly higher levels of mostly pancreatic serine proteases, such as trypsin and chymotrypsin-like elastase in V/M-treated (trypsin, 22-fold; chymotrypsin-like elastase, 9-fold increased) and GF mice (trypsin, 85-fold; chymotrypsin-like elastase, 28-fold increased) compared with untreated SPF mice (Figure 2*E*,

Figure 5. (***See previous page***). **Excessive large intestinal PA results in lasting impairment of the intestinal barrier in IL10$^{-/-}$ mice.** (*A*) Experimental setup: Untreated IL10$^{-/-}$ mice (ctr), V/M-treated IL10$^{-/-}$ mice at Day 2 of the treatment (V/M), and V/M-treated IL10$^{-/-}$ mice 7 days after discontinuation of the V/M treatment (post-V/M) were investigated. (*B*, *C*) Fecal and cecal serine protease activity. (*D*) Plasma concentration of fluorescein isothiocyanate dextran (4 kDa) 4 hours after oral gavage. (*E*) Ussing chamber analyses of cecal and colonic tissue. (*F*) mRNA expression level of IL1β and CD3 in colonic tissue. (*G*) Experimental schedule: V/M-treated IL10$^{-/-}$ mice were orally gavaged with the serine protease inhibitor AEBSF (V/M-AEBSF) or H_2O (V/M-wat), starting from 1 day before V/M treatment. (*H*, *I*) Fecal and cecal serine protease activity. (*J*) Plasma concentration of fluorescein isothiocyanate dextran (4 kDa) 4 hours after oral gavage. (*K*) Ussing chamber analyses of fluorescein translocation and TEER in colonic tissue sections. FITC, fluorescein isothiocyanate.

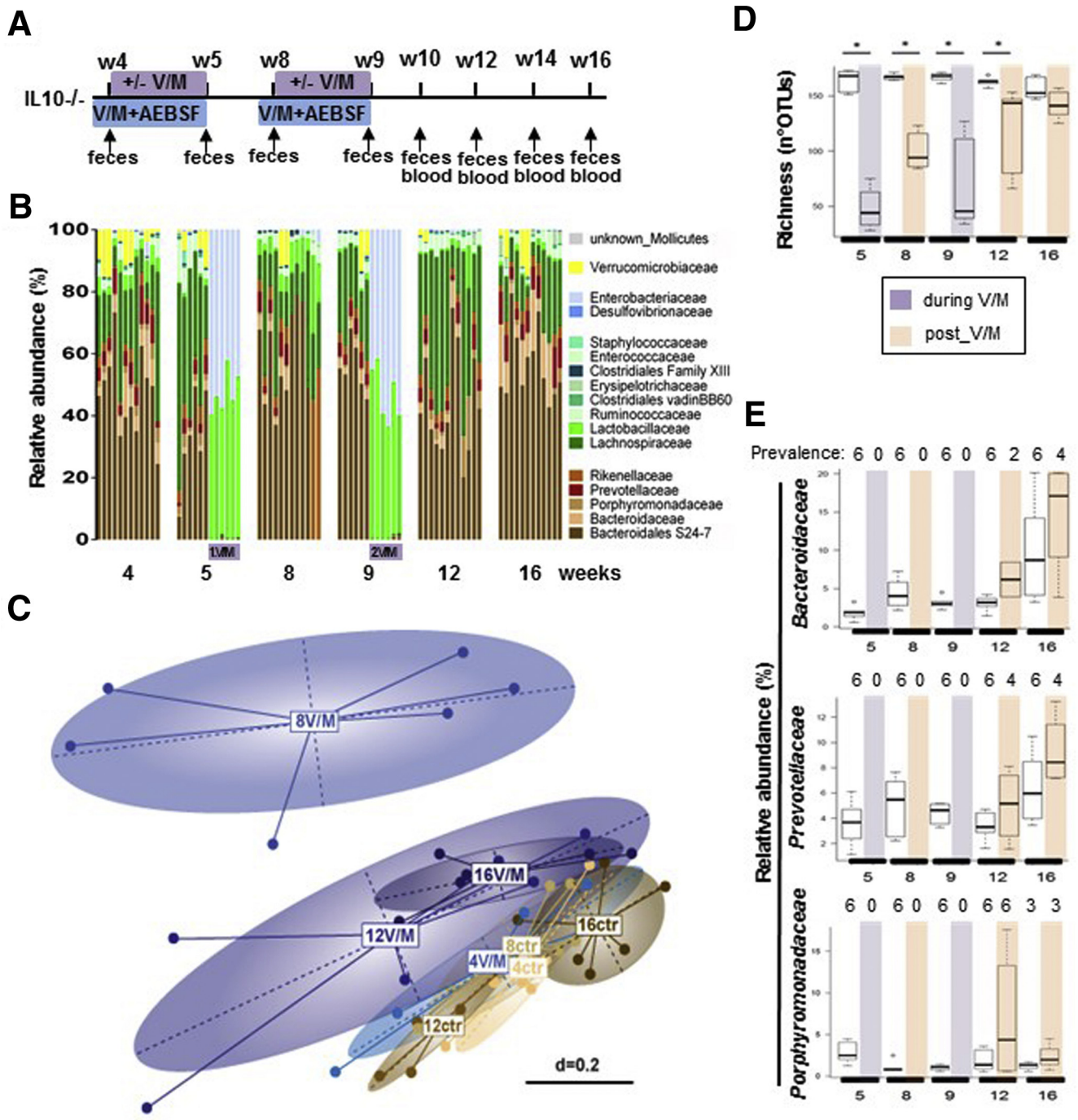

Figure 6. Impact of repeated V/M treatment on the microbial ecosystem in IL10$^{-/-}$ mice. (*A*) Long-term experimental setup: IL10$^{-/-}$ mice were left untreated or underwent repeated V/M treatment (2 times for 7 days at the age of 4 and 8 weeks) ± oral gavage of the serine protease inhibitor AEBSF (V/M-AEBSF) from 1 day before the beginning of the respective V/M treatment to Day 7. (*B*) Kinetic of the fecal microbiota composition in untreated versus V/M-treated IL10$^{-/-}$ mice (family level). (*C*) MetaNMDS plot showing fecal microbiota profiles (beta diversity) of untreated versus V/M-treated IL10$^{-/-}$ mice. (*D*) Microbial richness in ctr and V/M IL10$^{-/-}$ mice. Color code: *purple* = during V/M treatment, *light red* = post V/M treatment (after first and second V/M treatments). (*E*) Relative abundance of *Bacteroidaceae*, *Prevotellaceae*, and *Porphyromonadaceae* in untreated versus V/M-treated IL10$^{-/-}$ mice. The number of mice, in which the respective bacterial family was detected (prevalence) is depicted above the respective figure.

Supplementary Table 1). Of note, the abundance of bacterial proteases was found to be very low in comparison with host-derived proteases in ctr and V/M-treated mice, and none of the detected bacterial proteases was significantly increased on V/M-treatment (data not shown). Analogous to the results using patient stool-sup (Figure 1*C*), apical

exposure of PTK6 cells to cecal-sup from V/M-treated (Figure 2*F*) or GF (data not shown) mice resulted in significantly impaired epithelial barrier functions, whereas pretreatment with PMSF abrogated this detrimental effect. Furthermore, apical exposure of large intestinal tissue sections from SPF mice to high PA cecal-sup from GF mice resulted in significantly increased permeability and reduced TEER (Figure 2*G*), which was again abrogated by PMSF pretreatment of the cecal-sup. These findings clearly indicate that excess levels of pancreatic proteases are indeed detrimental to the large intestinal barrier function.

Excessive Large Intestinal Protease Activity Results in Transient Impairment of the Intestinal Barrier But No Significant Disturbance of the Intestinal Immune Homeostasis in Wild-Type Mice

V/M treatment of adult WT mice resulted in a rapid (Day 2) and lasting (Day 14: 7 days after discontinuation of ABx treatment) increase in large intestinal PA (Figure 3*A*–*C*). The rapid increase in PA was associated with significantly increased plasma levels of orally administered fluorescein isothiocyanate dextran (Figure 3*D*) and reduced *ex vivo* barrier functions of large intestinal tissue sections (Figure 3*E*). The integrity of the intestinal barrier was almost reestablished at Day 14 (Figure 3*D* and *E*) despite the lasting increase in PA, suggesting yet unknown adaptation mechanisms to restore the integrity of the intestinal barrier toward constantly increased PA. Interestingly, the V/M-induced transient leakage of the intestinal barrier affected neither the expression level of proinflammatory cytokines, such as IL1β (Figure 3*F*) or tumor necrosis factor (data not shown), nor markers for immune cell infiltration, such as CD3 (Figure 3*F*). This suggests an only minor impact of the high PA and the transiently increased permeability on the large intestinal immune homeostasis in WT mice.

Importantly, the rise in PA was found to be causal for the V/M-induced impairment of the intestinal barrier, because oral coadministration of the serine protease inhibitor AEBSF resulted in significantly reduced PA (Figure 3 *G*–*I*) and significant protection from the V/M-induced increase in mucosal permeability (Figure 3*J* and *K*).

To investigate whether the observed increase in PA and the concomitant transient impairment of the intestinal barrier results in increased vulnerability of the large intestinal immune homeostasis in the long term, WT mice underwent early and repeated V/M treatment followed by exposure to DSS 3 weeks after cessation of the second ABx treatment (Figure 4*A*). During each V/M course, microbial diversity was strongly reduced with *Lactobacillaceae* and *Enterobacteriaceae* being the dominant taxa (>99% relative abundance) (Figure 4*B*). Three weeks after cessation of the respective V/M course, the microbial composition was close to the pretreatment state at the level of dominant family composition. However, microbial diversity was still significantly reduced, which was mostly caused by the lasting eradication of families belonging to the order *Bacteroidales*, such as *Bacteroidaceae*, *Porphyromonadaceae*, and *Prevotellaceae* (Figure 4*C*–*E*), and the PA was still strongly increased in at least 50% of the mice (Figure 4*F*). However, these V/M-induced alterations did not promote the development of subsequent DSS-induced colitis (Figure 4*G*–*K*).

Excessive Large Intestinal Protease Activity Results in Lasting Impairment of the Intestinal Barrier in Interleukin $10^{-/-}$ Mice

Analogous to WT mice, V/M induced a rapid and lasting increase in PA in $IL10^{-/-}$ mice (Figure 5*A*–*C*), which was associated with significantly increased permeability of the intestinal barrier *in vivo* (Figure 5*D*) and significantly increased permeability of the large intestinal barrier *ex vivo* (Figure 5*E*). In contrast to WT mice, $IL10^{-/-}$ mice still showed a significant impairment of the intestinal barrier after the cessation of the ABx treatment (Figure 5*D* and *E*), indicating that the intestinal mucosa in $IL10^{-/-}$ mice is not able to cope with the persistently increased PA. In addition, $IL10^{-/-}$ mice showed significantly increased expression levels of IL1β (Figure 5*F*), tumor necrosis factor (data not shown), and CD3 (Figure 5*F*) already 7 days after cessation of the ABx treatment, suggesting that the increased permeability of the intestinal barrier triggers an inflammatory reaction in the large intestinal tissue. Importantly, oral coapplication of AEBSF during V/M-treatment was again found to reduce the rise in PA (Figure 5*G*–*I*) and to protect the intestinal barrier function (Figure 5*J* and *K*), demonstrating that the high PA is causal for the impaired intestinal barrier function in V/M-treated $IL10^{-/-}$ mice.

Excessive Large Intestinal Protease Activity Accelerates Colitis Development in Interleukin $10^{-/-}$ Mice

To determine the relevance of V/M-increased PA for the development of colitis in genetically susceptible organisms, $IL10^{-/-}$ mice underwent early and repeated V/M treatment with or without oral AEBSF cotreatment during the respective V/M course (Figure 6*A*). The V/M-induced alterations in the intestinal microbial ecosystem of $IL10^{-/-}$ mice were similar to the ones observed in WT mice (Figure 6*B*–*E*). The V/M-mediated rise in PA was significantly reduced by oral coadministration of AEBSF (Figure 7*A*). From the age of 14 weeks on, V/M-treated but not V/M-AEBSF cotreated $IL10^{-/-}$ mice showed significantly higher blood serum amyloid A and fecal complement component 3 (C3) levels compared with untreated control animals, indicating that the high PA accelerates colitis development (Figure 7*B* and *C*). Indeed, expression levels of inflammation markers, such as C3, IL1β, and interferon-γ, were significantly increased in the large intestinal tissue of V/M-treated $IL10^{-/-}$ mice compared with untreated or V/M-AEBSF cotreated $IL10^{-/-}$ mice (Figure 7*D*). Immunofluorescence analysis revealed significantly increased numbers of $CD3^{+}$ T cells in the large intestinal tissue of V/M-treated $IL10^{-/-}$ mice compared with untreated and V/M-AEBSF cotreated $IL10^{-/-}$ mice (Figure 7*E*). Histopathologic

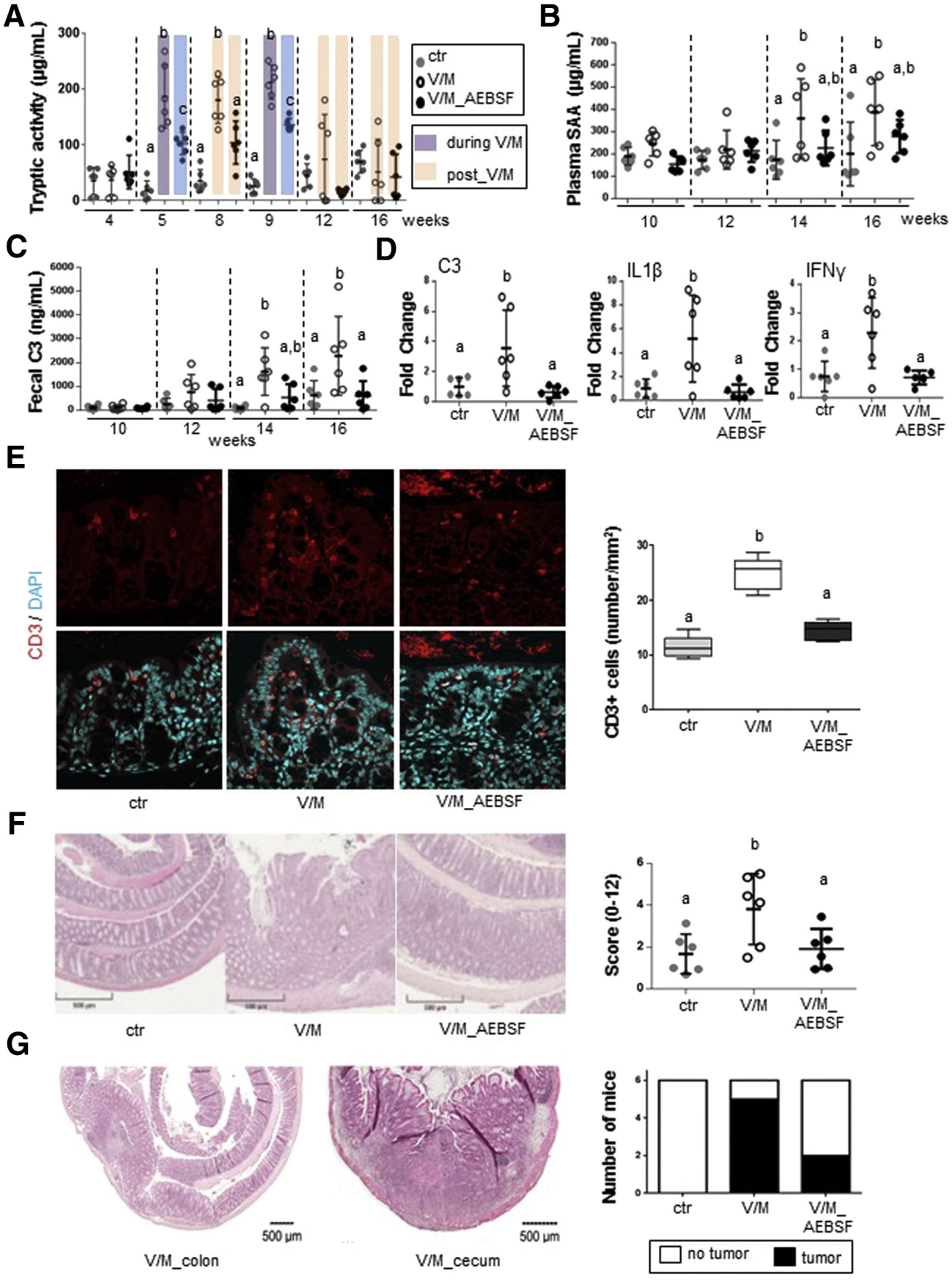
A
Tryptic activity (μg/mL)
ctr
V/M
V/M_AEBSF
during V/M
post_V/M
weeks
B
Plasma SAA (μg/mL)
weeks
C
Fecal C3 (ng/mL)
weeks
D
C3
IL1β
IFNγ
Fold Change
ctr
V/M
V/M_ AEBSF
E
CD3 / DAPI
ctr
V/M
V/M_AEBSF
CD3+ cells (number/mm²)
F
Score (0-12)
G
V/M_colon
V/M_cecum
500 μm
Number of mice
no tumor
tumor

analysis revealed significantly increased colitis severity in V/M-treated IL10$^{-/-}$ mice compared with untreated and V/M-AEBSF cotreated IL10$^{-/-}$ mice (Figure 7*F*). These findings demonstrate that the ABx-mediated rise in PA aggravates colitis in IL10$^{-/-}$ mice. Interestingly, in contrast to untreated IL10$^{-/-}$ mice, most V/M-treated IL10$^{-/-}$ mice (~80%) and some V/M-AEBSF cotreated IL10$^{-/-}$ mice (~30%) unexpectedly developed macroscopically visible large intestinal tumors already at 16 weeks of age (Figure 7*G*), indicating the ABx-mediated rise in PA to accelerate colitis-associated tumorigenesis.[60]

Discussion

The present study is the first to provide experimental evidence for the assumption that ABx therapies can trigger the development of chronic intestinal inflammation in genetically susceptible individuals. Excessive large intestinal PA, which is a frequently observed consequence of ABx therapy in patients, was identified to cause this severe adverse effect.

It has long been known that ABx treatment can abrogate the ability of the large intestinal microbiota to inactivate the high load of pancreatic proteases in the small intestinal content,[61,62] resulting in a major increase in large intestinal PA in rodents and human beings.[29-32] However, the physiological consequences of this adverse effect of ABx have been unknown. In our patient cohort, approximately a quarter of all patients showed a major (>5-fold) rise in stool PA on ABx treatment. All tested ABx classes mediated a major PA increase in some patients but not in others, demonstrating individual-specific vulnerability of the intestinal microbiota toward ABx therapies,[40,63,64] which is likely caused by the high interindividual variability of human microbial ecosystems. The fluoroquinolone ABx levofloxacin tended to confer a higher risk for a major PA rise than amoxicillin or rifaximin; however, this tendency needs to be confirmed in larger patient cohorts. In mice, oral treatment with V/M was consistently found to mediate an almost total loss of antiproteolytic activity in the large intestinal microbiota, indicating that the ABx mixture eradicates all antiproteolytic taxa. The inability of the intestinal microbiota from V/M-treated mice to inactivate serine proteases *ex vivo* or on transfer into GF mice supports the latter assumption. However, although our data are in line with published literature suggesting specific strains of the order *Bacteroidales* to play a role in the physiological inactivation of pancreatic proteases,[34,61,65] the identity of relevant antiproteolytic species/strains remains to be elucidated. The identification and isolation of antiproteolytic bacteria is challenging because the capacity to inactivate/degrade pancreatic proteases seems to be a rather rare bacterial function and none of the already investigated simplified microbial consortia (SIHUMIx,[62] altered Schaedler flora,[66] Oligo-MM community[67]; data not shown) are able to normalize the PA.

Although relevant microbes and molecular mechanisms remain to be discovered, the results of the present study demonstrate that the antiproteolytic activity of the large intestinal microbial ecosystem is of major importance for the integrity of the intestinal barrier. The rise in PA on V/M treatment resulted in significantly impaired intestinal barrier functions in WT and IL10$^{-/-}$ mice. Interestingly, the integrity of the intestinal barrier was rapidly restored in WT mice, despite constantly increased PA. In addition, the transient impairment of the intestinal barrier did not trigger a significant inflammatory activation of the large intestinal tissue in WT mice. It can be assumed that the observed adaptation of the large intestinal barrier to high PA levels is a physiological feedback mechanism to increased PA levels (as observed in diarrhea),[68,69] protecting the organism from lasting excess penetration of luminal microbes or microbe-associated molecular patterns. However, in contrast to healthy WT mice, colitis-susceptible IL10$^{-/-}$ mice were not able to restore the integrity of the intestinal barrier. Shortly after cessation of the ABx treatment, the lasting impairment of the intestinal barrier was paralleled by increased expression of inflammation markers in the large intestinal tissue, suggesting that the penetration of luminal antigens triggers proinflammatory mechanisms in genetically susceptible IL10$^{-/-}$ mice. The lasting impairment of the intestinal barrier may therefore be caused by the observed inflammatory activation of the large intestinal tissue, possibly affecting epithelial proliferation[70,71] and/or formation of tight and adherens junction complexes,[72,73] or vice versa. However, it can be assumed that these acute detrimental effects of the high PA on the large intestinal homeostasis cannot be controlled in colitis-susceptible IL10$^{-/-}$ mice, resulting in the observed high PA-mediated acceleration and aggravation of colitis development in V/M-treated IL10$^{-/-}$ mice. The finding that V/M-treated WT mice, despite lasting alterations in the intestinal microbial composition, high PA levels, and transiently reduced intestinal barrier functions, neither developed spontaneous colitis nor showed higher susceptibility toward DSS-induced colitis supports the

Figure 7. (*See previous page*). Excessive large intestinal PA accelerates colitis development in IL10$^{-/-}$ mice. (*A*) Kinetic of the fecal serine protease activity in IL10$^{-/-}$ mice. (*B*, *C*) Development of plasma serum amyloid A levels (systemic inflammation marker) and fecal complement component 3 (C3) levels (marker for intestinal inflammation) in IL10$^{-/-}$ mice. (*D*) mRNA expression levels of C3, IL1β, and interferon-γ in large intestinal tissue of IL10$^{-/-}$ mice. (*E*) T-cell infiltration in the proximal colon was determined by immunofluorescence staining of CD3^{+} cells. Quantification of CD3^{+} T cells per mm^2 at 6 representative regions in tissue sections per mouse. (*F*) The *left panel* shows representative pictures of hematoxylin-eosin-stained colonic tissue and the *right panel* shows the histopathologic score of individual IL10$^{-/-}$ mice. (*G*) The *left panel* shows representative pictures of hematoxylin-eosin-stained tumors that were exclusively observed in the cecum and colon of V/M-treated IL10$^{-/-}$ mice. The *right panel* shows the prevalence of tumor formation in the respective treatment group. IFN, interferon; SAA, serum amyloid A.

assumption that the intestinal barrier and immune functions in healthy organisms are well able to adapt to ABx-induced acute and long-term changes in the intestinal microbial ecosystem. This finding is in line with the fact that most ABx courses do not result in the development of chronic intestinal inflammation in patients.

In summary, the present study unravels significant detrimental effects of ABx-induced excess PA levels on the intestinal barrier and immune function in colitis-susceptible mice. Because a substantial fraction of ABx-treated patients shows an analogous rise in PA, it is highly probable that ABx treatment is not only associated[28] but indeed an independent risk factor for the development of chronic intestinal inflammation in IBD-susceptible individuals. It may be speculated that the high PA-mediated impairment of the large intestinal barrier might also play a role in the development of other chronic diseases that have been found to be associated with ABx therapies, such as irritable bowel syndrome[22,23] or colorectal cancer.[25,26] However, the pathophysiological impact of the rise in PA on the intestinal barrier in ABx-treated patients remains to be elucidated. With regard to IBD patients, the observed detrimental effects of ABx-induced high PA on the intestinal homeostasis, the lack of consistent clinical data supporting a protective effect of ABx therapy in IBD,[74] and the finding that ABx are associated with a more severe disease course and aggravated IBD-related microbial dysbiosis[13] suggest that ABx therapies rather contribute to the progression of the chronic inflammation. Finally, the present results support the development of innovative antiproteolytic strategies targeting the large intestinal PA (eg, oral administration of encapsulated serine protease inhibitors, commensal antiproteolytic bacteria, or genetically modified bacteria expressing protease inhibitors) to protect the large intestinal mucosa from adverse effects of ABx-induced or diarrhea-induced[35,38,69] high PA.

References

1. Sartor RB. Genetics and environmental interactions shape the intestinal microbiome to promote inflammatory bowel disease versus mucosal homeostasis. Gastroenterology 2010;139:1816–1819.
2. Sartor RB. Microbial influences in inflammatory bowel diseases. Gastroenterology 2008;134:577–594.
3. Jostins L, Ripke S, Weersma RK, Duerr RH, McGovern DP, Hui KY, Lee JC, Schumm LP, Sharma Y, Anderson CA, Essers J, Mitrovic M, Ning K, Cleynen I, Theatre E, Spain SL, Raychaudhuri S, Goyette P, Wei Z, Abraham C, Achkar JP, Ahmad T, Amininejad L, Ananthakrishnan AN, Andersen V, Andrews JM, Baidoo L, Balschun T, Bampton PA, Bitton A, Boucher G, Brand S, Büning C, Cohain A, Cichon S, D'Amato M, De Jong D, Devaney KL, Dubinsky M, Edwards C, Ellinghaus D, Ferguson LR, Franchimont D, Fransen K, Gearry R, Georges M, Gieger C, Glas J, Haritunians T, Hart A, Hawkey C, Hedl M, Hu X, Karlsen TH, Kupcinskas L, Kugathasan S, Latiano A, Laukens D, Lawrance IC, Lees CW, Louis E, Mahy G, Mansfield J, Morgan AR, Mowat C, Newman W, Palmieri O, Ponsioen CY, Potocnik U, Prescott NJ, Regueiro M, Rotter JI, Russell RK, Sanderson JD, Sans M, Satsangi J, Schreiber S, Simms LA, Sventoraityte J, Targan SR, Taylor KD, Tremelling M, Verspaget HW, De Vos M, Wijmenga C, Wilson DC, Winkelmann J, Xavier RJ, Zeissig S, Zhang B, Zhang CK, Zhao H, International IBD Genetics Consortium (IIBDGC), Silverberg MS, Annese V, Hakonarson H, Brant SR, Radford-Smith G, Mathew CG, Rioux JD, Schadt EE, Daly MJ, Franke A, Parkes M, Vermeire S, Barrett JC, Cho JH. Host-microbe interactions have shaped the genetic architecture of inflammatory bowel disease. Nature 2012;491:119–124.
4. Khor B, Gardet A, Xavier RJ. Genetics and pathogenesis of inflammatory bowel disease. Nature 2011;474:307–317.
5. Strober W, Fuss I, Mannon P. The fundamental basis of inflammatory bowel disease. J Clin Invest 2007;117:514–521.
6. Maloy KJ, Powrie F. Intestinal homeostasis and its breakdown in inflammatory bowel disease. Nature 2011;474:298–306.
7. Heller F, Florian P, Bojarski C, Richter J, Christ M, Hillenbrand B, Mankertz J, Gitter AH, Bürgel N, Fromm M, Zeitz M, Fuss I, Strober W, Schulzke JD. Interleukin-13 is the key effector Th2 cytokine in ulcerative colitis that affects epithelial tight junctions, apoptosis, and cell restitution. Gastroenterology 2005;129:550–564.
8. Liu JZ, van Sommeren S, Huang H, Ng SC, Alberts R, Takahashi A, Ripke S, Lee JC, Jostins L, Shah T, Abedian S, Cheon JH, Cho J, Dayani NE, Franke L, Fuyuno Y, Hart A, Juyal RC, Juyal G, Kim WH, Morris AP, Poustchi H, Newman WG, Midha V, Orchard TR, Vahedi H, Sood A, Sung JY, Malekzadeh R, Westra HJ, Yamazaki K, Yang SK, International Multiple Sclerosis Genetics Consortium, International IBD Genetics Consortium, Barrett JC, Alizadeh BZ, Parkes M, Bk T, Daly MJ, Kubo M, Anderson CA, Weersma RK. Association analyses identify 38 susceptibility loci for inflammatory bowel disease and highlight shared genetic risk across populations. Nat Genet 2015;47:979–986.
9. Ananthakrishnan AN. Epidemiology and risk factors for IBD. Nat Rev Gastroenterol Hepatol 2015;12:205–217.
10. Kaser A, Zeissig S, Blumberg RS. Inflammatory bowel disease. Annu Rev Immunol 2010;28:573–621.
11. Huttenhower C, Kostic AD, Xavier RJ. Inflammatory bowel disease as a model for translating the microbiome. Immunity 2014;40:843–854.
12. Schaubeck M, Clavel T, Calasan J, Lagkouvardos I, Haange SB, Jehmlich N, Basic M, Dupont A, Hornef M, von Bergen M, Bleich A, Haller D. Dysbiotic gut microbiota causes transmissible Crohn's disease-like ileitis independent of failure in antimicrobial defense. Gut 2016;65:225–237.
13. Gevers D, Kugathasan S, Denson LA, Vázquez-Baeza Y, Van Treuren W, Ren B, Schwager E, Knights D, Song SJ, Yassour M, Morgan XC, Kostic AD, Luo C, González A, McDonald D, Haberman Y, Walters T, Baker S, Rosh J, Stephens M, Heyman M, Markowitz J, Baldassano R, Griffiths A, Sylvester F, Mack D, Kim S, Crandall W,

Hyams J, Huttenhower C, Knight R, Xavier RJ. The treatment-naive microbiome in new-onset Crohn's disease. Cell Host Microbe 2014;15:382–392.
14. Tremaroli V, Bäckhed F. Functional interactions between the gut microbiota and host metabolism. Nature 2012; 489:242–249.
15. Buffie CG, Pamer EG. Microbiota-mediated colonization resistance against intestinal pathogens. Nat Rev Immunol 2013;13:790–801.
16. Hooper LV, Gordon JI. Commensal host-bacterial relationships in the gut. Science 2001;292:1115–1118.
17. Macfarlane GT, Macfarlane S. Human colonic microbiota: ecology, physiology and metabolic potential of intestinal bacteria. Scand J Gastroenterol Suppl 1997; 222:3–9.
18. Schulfer AF, Battaglia T, Alvarez Y, Bijnens L, Ruiz VE, Ho M, Robinson S, Ward T, Cox LM, Rogers AB, Knights D, Sartor RB, Blaser MJ. Intergenerational transfer of antibiotic-perturbed microbiota enhances colitis in susceptible mice. Nat Microbiol 2018;3:234–242.
19. Willing BP, Russell SL, Finlay BB. Shifting the balance: antibiotic effects on host-microbiota mutualism. Nat Rev Microbiol 2011;9:233–243.
20. Dalal SR, Chang EB. The microbial basis of inflammatory bowel diseases. J Clin Invest 2014;124:4190–4196.
21. Nobel YR, Cox LM, Kirigin FF, Bokulich NA, Yamanishi S, Teitler I, Chung J, Sohn J, Barber CM, Goldfarb DS, Raju K, Abubucker S, Zhou Y, Ruiz VE, Li H, Mitreva M, Alekseyenko AV, Weinstock GM, Sodergren E, Blaser MJ. Metabolic and metagenomic outcomes from early-life pulsed antibiotic treatment. Nat Commun 2015; 6:7486.
22. Maxwell PR, Rink E, Kumar D, Mendall MA. Antibiotics increase functional abdominal symptoms. Am J Gastroenterol 2002;97:104–108.
23. Mendall MA, Kumar D. Antibiotic use, childhood affluence and irritable bowel syndrome (IBS). Eur J Gastroenterol Hepatol 1998;10:59–62.
24. Wang JL, Chang CH, Lin JW, Wu LC, Chuang LM, Lai MS. Infection, antibiotic therapy and risk of colorectal cancer: a nationwide nested case-control study in patients with type 2 diabetes mellitus. Int J Cancer 2014; 135:956–967.
25. Dik VK, van Oijen MG, Smeets HM, Siersema PD. Frequent use of antibiotics is associated with colorectal cancer risk: results of a nested case-control study. Dig Dis Sci 2016;61:255–264.
26. Korpela K, Salonen A, Virta L, Kekkonen RA, Forslund K, Bork P, de Vos WM. Intestinal microbiome is related to lifetime antibiotic use in Finnish pre-school children. Nat Commun 2016;7:10410.
27. Hviid A, Svanström H, Frisch M. Antibiotic use and inflammatory bowel diseases in childhood. Gut 2011; 60:49–54.
28. Ungaro R, Bernstein CN, Gearry R, Hviid A, Kolho KL, Kronman MP, Shaw S, Van Kruiningen H, Colombel JF, Atreja A. Antibiotics associated with increased risk of new-onset Crohn's disease but not ulcerative colitis: a meta-analysis. Am J Gastroenterol 2014;109:1728–1738.
29. Genell S, Gustafsson BE. Impaired enteric degradation of pancreatic endopeptidases in antibiotic-treated rats. Scand J Gastroenterol 1977;12:801–809.
30. Carlstedt-Duke B, Gustafsson BE, Midtvedt T. Clindamycin-induced alterations in intestinal microflora-associated characteristics in rats. Scand J Gastroenterol 1985;20:92–98.
31. Bohe M, Borgstrom A, Genell S, Ohlsson K. Determination of immunoreactive trypsin, pancreatic elastase and chymotrypsin in extracts of human feces and ileostomy drainage. Digestion 1983;27:8–15.
32. Borgstrom A, Genell S, Ohlsson K. Elevated fecal levels of endogenous pancreatic endopeptidases after antibiotic treatment. Scand J Gastroenterol 1977; 12:525–529.
33. Macfarlane GT, Allison C, Gibson SA, Cummings JH. Contribution of the microflora to proteolysis in the human large intestine. J Appl Bacteriol 1988;64:37–46.
34. Carroll IM, Ringel-Kulka T, Ferrier L, Wu MC, Siddle JP, Bueno L, Ringel Y. Fecal protease activity is associated with compositional alterations in the intestinal microbiota. PLoS One 2013;8:e78017.
35. Gecse K, Róka R, Ferrier L, Leveque M, Eutamene H, Cartier C, Ait-Belgnaoui A, Rosztóczy A, Izbéki F, Fioramonti J, Wittmann T, Bueno L. Increased faecal serine protease activity in diarrhoeic IBS patients: a colonic lumenal factor impairing colonic permeability and sensitivity. Gut 2008;57:591–599.
36. Antalis TM, Shea-Donohue T, Vogel SN, Sears C, Fasano A. Mechanisms of disease: protease functions in intestinal mucosal pathobiology. Nat Clin Pract Gastroenterol Hepatol 2007;4:393–402.
37. Zeissig S, Bürgel N, Günzel D, Richter J, Mankertz J, Wahnschaffe U, Kroesen AJ, Zeitz M, Fromm M, Schulzke JD. Changes in expression and distribution of claudin 2, 5 and 8 lead to discontinuous tight junctions and barrier dysfunction in active Crohn's disease. Gut 2007;56:61–72.
38. Kiesslich R, Duckworth CA, Moussata D, Gloeckner A, Lim LG, Goetz M, Pritchard DM, Galle PR, Neurath MF, Watson AJ. Local barrier dysfunction identified by confocal laser endomicroscopy predicts relapse in inflammatory bowel disease. Gut 2012;61:1146–1153.
39. Hansen KK, Sherman PM, Cellars L, Andrade-Gordon P, Pan Z, Baruch A, Wallace JL, Hollenberg MD, Vergnolle N. A major role for proteolytic activity and proteinase-activated receptor-2 in the pathogenesis of infectious colitis. Proc Natl Acad Sci U S A 2005; 102:8363–8368.
40. Panda S, El khader I, Casellas F, López Vivancos J, García Cors M, Santiago A, Cuenca S, Guarner F, Manichanh C. Short-term effect of antibiotics on human gut microbiota. PLoS One 2014;18:9.
41. Shevchenko A, Tomas H, Havlis J, Olsen JV, Mann M. In-gel digestion for mass spectrometric characterization of proteins and proteomes. Nat Protoc 2006;1: 2856–2860.
42. Hahne H, Pachl F, Ruprecht B, Maier SK, Klaeger S, Helm D, Médard G, Wilm M, Lemeer S, Kuster B. DMSO

enhances electrospray response, boosting sensitivity of proteomic experiments. Nat Methods 2013;10:989–991.
43. Cox J, Mann M. MaxQuant enables high peptide identification rates, individualized p.p.b.-range mass accuracies and proteome-wide protein quantification. Nat Biotechnol 2008;26:1367–1372.
44. Cox J, Neuhauser N, Michalski A, Scheltema RA, Olsen JV, Mann M. Andromeda: a peptide search engine integrated into the MaxQuant environment. J Proteome Res 2011;10:1794–1805.
45. Cox J, Hein MY, Luber CA, Paron I, Nagaraj N, Mann M. Accurate proteome-wide label-free quantification by delayed normalization and maximal peptide ratio extraction, termed MaxLFQ. Mol Cell Proteomics 2014; 13:2513–2526.
46. Tyanova S, Temu T, Sinitcyn P, Carlson A, Hein MY, Geiger T, Mann M, Cox J. The Perseus computational platform for comprehensive analysis of (prote)omics data. Nat Methods 2016;13:731–740.
47. Rutgeerts P, Van Assche G, Vermeire S, D'Haens G, Baert F, Noman M, Aerden I, De Hertogh G, Geboes K, Hiele M, D'Hoore A, Penninckx F. Ornidazole for prophylaxis of postoperative Crohn's disease recurrence: a randomized, double-blind, placebo-controlled trial. Gastroenterology 2005;128:856–861.
48. Katakura K, Lee J, Rachmilewitz D, Li G, Eckmann L, Raz E. Toll-like receptor 9-induced type I IFN protects mice from experimental colitis. J Clin Invest 2005; 115:695–702.
49. Godon JJ, Zumstein E, Dabert P, Habouzit F, Moletta R. Molecular microbial diversity of an anaerobic digestor as determined by small-subunit Rdna sequence analysis. Appl Environ Microbiol 1997;63:2802–2813.
50. Lagkouvardos I, Klaring K, Heinzmann S, Platz S, Scholz B, Engel KH, Schmitt-Kopplin P, Haller D, Rohn S, Skurk T, Clavel T. Gut metabolites and bacterial community networks during a pilot intervention study with flaxseeds in healthy adult men. Mol Nutr Food Res 2015; 59:1614–1628.
51. Berry D, Ben Mahfoudh K, Wagner M, Loy A. Barcoded primers used in multiplex amplicon pyrosequencing bias amplification. Appl Environ Microbiol 2011;77: 7846–7849.
52. Klindworth A, Pruesse E, Schweer T, Peplies J, Quast C, Horn M, Glöckner FO. Evaluation of general 16S ribosomal RNA gene PCR primers for classical and next-generation sequencing-based diversity studies. Nucleic Acids Res 2013;41:e1.
53. Lagkouvardos I, Joseph D, Kapfhammer M, Giritli S, Horn M, Haller D, Clavel T. IMNGS: A massive open resource of processed 16S rRNA microbial profiles for ecology and diversity studies. Sci Rep 2016;6:33721.
54. Edgar RC. UPARSE: highly accurate OTU sequences from microbial amplicon reads. Nat Methods 2013; 10:996–998.
55. Edgar RC, Haas BJ, Clemente JC, Quince C, Knight R. UCHIME improves sensitivity and speed of chimera detection. Bioinformatics 2011;27:2194–2200.
56. Wang Q, Garrity GM, Tiedje JM, Cole JR. Naive Bayesian classifier for rapid assignment of rRNA sequences into the new bacterial taxonomy. Appl Environ Microbiol 2007;73:5261–5267.
57. Lagkouvardos I, Fischer S, Kumar N, Clavel T. Rhea: a transparent and modular R pipeline for microbial profiling based on 16S rRNA gene amplicons. PeerJ 2017;5:e2836.
58. Chen J, Bittinger K, Charlson ES, Hoffmann C, Lewis J, Wu GD, Collman RG, Bushman FD, Li H. Associating microbiome composition with environmental covariates using generalized UniFrac distances. Bioinformatics 2012;28:2106–2113.
59. Jost L. Partitioning diversity into independent alpha and beta components. Ecology 2007;88:2427–2439.
60. Berg DJ, Davidson N, Kühn R, Müller W, Menon S, Holland G, Thompson-Snipes L, Leach MW, Rennick D. Enterocolitis and colon cancer in interleukin-10-deficient mice are associated with aberrant cytokine production and CD4(+) TH1-like responses. J Clin Invest 1996; 98:1010–1020.
61. Ramare F, Hautefort I, Verhe F, Raibaud P, Iovanna J. Inactivation of tryptic activity by a human-derived strain of *Bacteroides distasonis* in the large intestines of gnotobiotic rats and mice. Appl Environ Microbiol 1996; 62:1434–1436.
62. Becker N, Kunath J, Loh G, Blaut M. Human intestinal microbiota: characterization of a simplified and stable gnotobiotic rat model. Gut Microbes 2011;2:25–33.
63. DuPont HL. Review article: the antimicrobial effects of rifaximin on the gut microbiota. Aliment Pharmacol Ther 2016;43(Suppl 1):3–10.
64. Dethlefsen L, Relman DA. Incomplete recovery and individualized responses of the human distal gut microbiota to repeated antibiotic perturbation. Proc Natl Acad Sci U S A 2011;108(Suppl 1):4554–4561.
65. Midtvedt T, Zabarovsky E, Norin E, Bark J, Gizatullin R, Kashuba V, Ljungqvist O, Zabarovska V, Möllby R, Ernberg I. Increase of faecal tryptic activity relates to changes in the intestinal microbiome: analysis of Crohn's disease with a multidisciplinary platform. PLoS One 2013;8:e66074.
66. Norin E, Midtvedt T. Intestinal microflora functions in laboratory mice claimed to harbor a "normal" intestinal microflora. Is the SPF concept running out of date? Anaerobe 2010;16:311–313.
67. Brugiroux S, Beutler M, Pfann C, Garzetti D, Ruscheweyh HJ, Ring D, Diehl M, Herp S, Lötscher Y, Hussain S, Bunk B, Pukall R, Huson DH, Münch PC, McHardy AC, McCoy KD, Macpherson AJ, Loy A, Clavel T, Berry D, Stecher B. Genome-guided design of a defined mouse microbiota that confers colonization resistance against *Salmonella enterica* serovar *Typhimurium*. Nat Microbiol 2016;2:16215.
68. Tooth D, Garsed K, Singh G, Marciani L, Lam C, Fordham I, Fields A, Banwait R, Lingaya M, Layfield R, Hastings M, Whorwell P, Spiller R. Characterisation of faecal protease activity in irritable bowel syndrome with diarrhoea: origin and effect of gut transit. Gut 2014; 63:753–760.

69. Róka R, Rosztóczy A, Leveque M, Izbéki F, Nagy F, Molnár T, Lonovics J, Garcia-Villar R, Fioramonti J, Wittmann T, Bueno L. A pilot study of fecal serine-protease activity: a pathophysiologic factor in diarrhea-predominant irritable bowel syndrome. Clin Gastroenterol Hepatol 2007;5:550–555.
70. Kaiser GC, Polk DB. Tumor necrosis factor alpha regulates proliferation in a mouse intestinal cell line. Gastroenterology 1997;112:1231–1240.
71. Ruemmele FM, Gurbindo C, Mansour AM, Marchand R, Levy E, Seidman EG. Effects of interferon gamma on growth, apoptosis, and MHC class II expression of immature rat intestinal crypt (IEC-6) cells. J Cell Physiol 1998;176:120–126.
72. Bruewer M, Samarin S, Nusrat A. Inflammatory bowel disease and the apical junctional complex. Ann N Y Acad Sci 2006;1072:242–252.
73. Capaldo CT, Nusrat A. Cytokine regulation of tight junctions. Biochim Biophys Acta 2009;1788:864–871.
74. Sartor RB. Therapeutic manipulation of the enteric microflora in inflammatory bowel diseases: antibiotics, probiotics, and prebiotics. Gastroenterology 2004;126:1620–1633.

Received December 12, 2017. Accepted May 15, 2018.

Correspondence
Address correspondence to: Dirk Haller, PhD, Chair of Nutrition and Immunology, Gregor-Mendel-Str.2, 85350 Freising-Weihenstephan, Germany. e-mail: dirk.haller@tum.de; or Gabriele Hörmannsperger, PhD, Chair of Nutrition and Immunology, Gregor-Mendel-Str.2, 85350 Freising-Weihenstephan, Germany. e-mail: gabriele.hoermannsperger@tum.de.

Acknowledgements
The authors thank Sigrid Kisling and Silvia Pitariu for histopathologic scoring; Alexandra Buse, Felicitas Firlus, and Caroline Ziegler for outstanding technical assistance; and Valentina Schüppel for support with Ussing chamber assays.

Hongsup Yoon and Gabriele Hörmannsperger designed the experiments. Hongsup Yoon, Monika Schaubeck, and Gabriele Hörmannsperger performed experiments. Suchita Panda, Chaysavanh Manichanh, Patrizia Kump, and Andreas Blesl provided patient stool samples. Ilias Lagkouvardos and Thomas Clavel performed 16S rRNA gene amplicon analysis. Andreas Blesl, Christina Ludwig, Hannes Hahne, and Bernhard Küster performed LC-MS/MS analysis. Hongsup Yoon and Gabriele Hörmannsperger wrote the manuscript. Monika Schaubeck, Ilias Lagkouvardos, Thomas Clavel, and Dirk Haller provided intellectual input and reviewed the manuscript intensively. All authors approved the final version of the manuscript.

Conflicts of interest
The authors disclose no conflicts.

Funding
This work was financed by the Deutscher Akademischer Austauschdienst, and supported by the Technische Universität München Graduate School.

Supplementary Table 1. Abundance of Proteases and Protease Inhibitors in Cecal-Sup of Untreated, V/M-Treated, and GF WT Mice (Determined Via LC-MS/MS Analysis)

Protein names	Gene names	Identified number	MS/MS count	Category	Average intensity (log2 iBAQ)			Ratio (V/M vs ctrl)	Ratio (GF vs ctrl)	*P* value (V/M vs ctrl)	*P* value (GF vs ctrl)
					Ctrl mice	V/M mice	GF mice				
Anionic trypsin-2	Prss2	11	6463	s.p.	23.58	28.04	30.00	22.11	85.74	9.5E-05	3.0E-05
Chymotrypsin-like elastase family member 3B	Cela3b	14	5278	s.p.	23.53	26.73	28.36	9.15	28.29	1.7E-02	4.9E-03
Chymotrypsin-like elastase family member 2A	Cela2a	6	190	s.p.	21.77	21.71	20.39	0.96	0.38	9.5E-01	3.3E-01
Chymotrypsin B	Ctrb1	6	110	s.p.	19.56	22.05	20.56	5.64	2.01	3.8E-03	9.5E-03
Dipeptidyl-peptidase 4	Dpp4	28	536	s.p.	18.10	19.65	20.82	2.93	6.61	4.1E-02	7.9E-02
Enteropeptidase;	Tmprss15	16	182	s.p.	13.90	16.72	19.60	7.04	51.88	1.2E-01	1.3E-02
Serine protease 30	Prss30	3	33	s.p.	16.53	16.83	18.74	1.23	4.64	5.1E-01	3.7E-03
Suppressor of tumorigenicity 14 protein homolog	St14	5	29	s.p.	15.04	15.95	15.88	1.87	1.79	7.6E-02	1.9E-01
Heat shock protein HSP 90-beta	Hsp90ab1	4	16	s.p.	16.16	12.60	14.66	0.09	0.36	—	6.5E-01
Lysosomal protective protein	Ctsa	6	31	s.p.	15.96	NaN	15.54	—	0.75	9.3E-02	8.7E-01
Lysosomal Pro-X carboxypeptidase	Prcp	3	13	s.p.	16.05	13.31	13.47	0.15	0.17	4.6E-02	3.1E-02
Haptoglobin	Hp	9	48	s.p.	15.85	14.04	NaN	0.29	—	1.0E-01	7.4E-02
Transmembrane protease serine 2	Tmprss2	3	10	s.p.	NaN	NaN	14.99	—	—	—	3.7E-02
Kallikrein 1-related peptidase b22	Klk1b22	3	16	s.p.	14.64	19.27	NaN	24.91	—	—	—
Mast cell protease 2	Mcpt2	5	15	s.p.	17.62	NaN	15.28	—	0.20	4.1E-02	1.9E-01
Acylamino-acid-releasing enzyme	Apeh	1	7	s.p.	15.50	12.04	NaN	0.09	—	—	—
Mast cell protease 1	Mcpt1	6	22	s.p.	20.58	NaN	NaN	—	—	7.1E-02	1.3E-01
Prolyl endopeptidase	Prep	6	24	s.p.	16.09	NaN	NaN	—	—	3.5E-02	3.3E-02
Lactotransferrin	Ltf	7	18	s.p.	NaN	NaN	NaN	—	—	—	—
Proteasome subunit beta type-5	Psmb5	10	56	t.p.	18.65	14.18	18.57	0.04	0.94	1.0E-02	9.3E-01
γ-Glutamyltranspeptidase 1	Ggt1	10	171	t.p.	12.08	18.57	18.39	89.57	78.90	2.1E-03	1.0E-01
N(4)-(β-N-acetylglucosaminyl)-L-asparaginase	Aga	5	50	t.p.	14.40	14.35	18.54	0.96	17.63	5.9E-01	2.0E-03
Proteasome subunit alpha type-1	Psma1	11	57	t.p.	17.99	11.90	17.58	0.01	0.75	2.0E-03	6.8E-01
Proteasome subunit alpha type-3	Psma3	9	34	t.p.	18.49	9.15	18.72	0.00	1.17	2.1E-03	8.5E-01
Proteasome subunit alpha type-4	Psma4	6	48	t.p.	18.39	10.42	18.44	0.00	1.04	1.3E-02	9.8E-01
Proteasome subunit alpha type-2	Psma2	8	46	t.p.	18.44	11.08	16.70	0.01	0.30	1.3E-03	1.7E-01
Proteasome subunit alpha type-5	Psma5	5	54	t.p.	18.84	NaN	18.77	—	0.95	1.3E-03	4.0E-01
Proteasome subunit beta type-6	Psmb6	3	39	t.p.	18.21	NaN	17.90	—	0.80	1.3E-02	8.3E-01
Proteasome subunit alpha type-7	Psma7	9	64	t.p.	19.25	NaN	17.82	—	0.37	5.0E-03	2.5E-01
Proteasome subunit beta type-2	Psmb2	6	42	t.p.	17.99	NaN	18.57	—	1.50	1.1E-02	6.8E-01

Supplementary Table 1. Continued

Protein names	Gene names	Identified number	MS/MS count	Category	Average intensity (log2 iBAQ)			Ratio (V/M vs ctrl)	Ratio (GF vs ctrl)	*P* value (V/M vs ctrl)	*P* value (GF vs ctrl)
					Ctrl mice	V/M mice	GF mice				
Proteasome subunit beta type-1	Psmb1	6	34	t.p.	18.91	NaN	17.61	—	0.41	1.2E-03	4.1E-01
Proteasome subunit alpha type-6	Psma6	9	69	t.p.	19.20	NaN	17.44	—	0.30	6.2E-04	1.8E-01
Proteasome subunit beta type-3	Psmb3	3	12	t.p.	17.12	NaN	18.27	—	2.23	—	2.0E-01
Proteasome subunit beta type-4	Psmb4	5	30	t.p.	18.94	NaN	NaN	—	—	4.9E-03	4.7E-03
Proteasome subunit beta type-8	Psmb8	4	11	t.p.	15.41	11.69	NaN	0.08	—	—	—
Proteasome subunit beta type-10	Psmb10	3	13	t.p.	16.75	NaN	NaN	—	—	4.0E-03	1.8E-02
Proteasome subunit beta type-7	Psmb7	2	6	t.p.	16.44	NaN	NaN	—	—	1.9E-02	2.1E-02
Transthyretin	Ttr	12	785	a.p.	21.46	20.68	19.73	0.58	0.30	1.6E-01	2.8E-02
N-acetylated-alpha-linked acidic dipeptidase-like protein	Naaladl1	33	1930	a.p.	16.44	NaN	NaN	—	—	4.2E-03	2.0E-02
Aminopeptidase N	Anpep	57	2258	c.p.	18.14	19.83	21.51	3.23	10.32	4.3E-03	4.2E-04
Carboxypeptidase A1	Cpa1	16	704	c.p.	18.30	16.61	18.03	0.31	0.83	6.0E-02	8.5E-01
Meprin A subunit beta	Mep1b	25	1168	c.p.	16.80	14.03	17.52	0.15	1.64	2.8E-01	6.6E-01
Meprin A subunit alpha	Mep1a	18	687	c.p.	16.50	NaN	16.56	—	1.04	—	—
Glutamyl aminopeptidase	Enpep	49	1225	c.p.	15.34	16.60	15.49	2.39	1.11	1.0E-01	5.0E-01
Angiotensin-converting enzyme	Ace	43	532	c.p.	NaN	NaN	13.58	—	—	—	5.8E-01
Dipeptidase 1	Dpep1	12	165	c.p.	16.50	11.70	NaN	0.04	—	5.9E-03	4.8E-03
Carboxypeptidase Q	Cpq	10	116	c.p.	15.58	NaN	NaN	—	—	9.5E-02	1.2E-01
Angiotensin-converting enzyme 2	Ace2	27	472	m.p.	21.29	24.03	24.73	6.65	10.88	6.3E-02	4.2E-02
Carboxypeptidase A2	Cpa2	7	42	m.p.	19.18	23.25	24.70	16.83	46.03	3.8E-03	1.0E-02
Aspartyl aminopeptidase	Dnpep	6	17	m.p.	19.80	23.14	24.35	10.10	23.34	1.4E-02	1.7E-02
Cytosol aminopeptidase	Lap3	10	36	m.p.	22.93	22.76	22.52	0.89	0.75	9.3E-01	8.3E-01
Cytochrome b-c1 complex subunit 2, mitochondrial	Uqcrc2	1	1	m.p.	19.41	22.62	23.87	9.26	21.99	9.8E-03	1.1E-02
Dipeptidyl peptidase 3	Dpp3	3	5	m.p.	15.75	20.54	22.60	27.63	114.71	1.7E-02	5.6E-03
Cathepsin S	Ctss	12	211	m.p.	15.62	20.54	21.98	30.21	82.05	6.2E-03	2.0E-02
γ-Glutamyl hydrolase	Ggh	7	108	m.p.	18.53	21.09	20.27	5.91	3.35	5.4E-03	5.0E-01
Cathepsin B	Ctsb	9	36	m.p.	15.81	20.35	20.86	23.26	33.16	3.5E-03	4.7E-02
Dipeptidyl-peptidase 1	Ctsc	1	22	m.p.	16.79	20.24	20.79	10.92	15.98	1.8E-02	8.3E-02
Bleomycin hydrolase	Blmh	3	15	m.p.	16.61	16.38	20.20	0.85	12.01	6.0E-01	4.4E-04
Procathepsin H	Ctsh	2	3	m.p.	14.38	17.12	20.43	6.71	66.37	1.7E-02	2.2E-03
Calpain-5	Capn5	4	5	m.p.	14.09	20.91	21.41	113.31	159.40	2.9E-03	2.1E-02
Caspase-7 subunit	Casp7	3	12	m.p.	21.08	15.30	15.23	0.02	0.02	4.1E-01	2.1E-01
Calpain-1 catalytic subunit	Capn1	6	29	m.p.	15.30	17.43	NaN	4.40	—	2.4E-02	—
Ubiquitin carboxyl-terminal hydrolase 14	Usp14	1	2	m.p.	15.80	17.31	13.83	2.84	0.26	7.2E-02	1.0E-01
Cathepsin D	Ctsd	2	14	m.p.	15.30	NaN	NaN	—	—	2.7E-02	3.2E-02
α_1-Antitrypsin 1-2	Serpina1b	24	1044	p.i.	23.08	22.44	23.74	0.64	1.58	5.0E-01	2.9E-01
Serine protease inhibitor A3K	Serpina3k	27	1256	p.i.	22.32	21.77	24.10	0.68	3.42	6.0E-01	7.4E-02

Supplementary Table 1. Continued

Protein names	Gene names	Identified number	MS/MS count	Category	Average intensity (log2 iBAQ)			Ratio (V/M vs ctrl)	Ratio (GF vs ctrl)	*P* value (V/M vs ctrl)	*P* value (GF vs ctrl)
					Ctrl mice	V/M mice	GF mice				
α_1-Antitrypsin 1-4	Serpina1d	9	421	p.i.	20.31	21.21	22.23	1.87	3.79	3.5E-01	8.1E-02
Serine protease inhibitor A3M	Serpina3m	2	28	p.i.	20.47	21.35	19.67	1.83	0.57	4.9E-01	7.8E-01
Leukocyte elastase inhibitor A	Serpinb1a	28	861	p.i.	22.28	19.09	22.87	0.11	1.51	1.3E-03	2.6E-01
α_1-Antitrypsin 1-3	Serpina1c	6	454	p.i.	20.50	19.72	22.27	0.27	0.53	3.0E-01	6.6E-01
α_1-Antitrypsin 1-5	Serpina1e	9	169	p.i.	19.94	18.07	19.02	0.09	1.72	5.4E-03	3.1E-01
Cystatin-B	Cstb	5	82	p.i.	20.38	16.98	21.17	0.58	2.36	3.4E-01	4.2E-02
Antithrombin-III	Serpinc1	15	170	p.i.	18.17	17.39	19.41	0.61	4.29	4.6E-01	1.6E-01
α_2-Macroglobulin	A2m	33	280	p.i.	16.84	16.12	18.94	1.20	7.30	8.7E-01	4.0E-02
Murinoglobulin-1	Mug1	21	243	p.i.	15.74	16.01	18.61	0.55	65.52	—	9.8E-04
Serpin B12	Serpinb12	11	126	p.i.	13.59	12.72	19.63	0.13	1.11	9.1E-02	8.9E-01
Serine protease inhibitor A3N	Serpina3n	5	43	p.i.	17.12	14.16	17.27	0.62	2.89	—	7.8E-02
α_2-Antiplasmin	Serpinf2	3	12	p.i.	15.07	14.37	16.60	0.25	0.12	4.4E-02	1.6E-02
α_1-Microglobulin	Ambp	2	12	p.i.	NaN	13.90	14.70	1.31	—	1.2E-01	—
Submaxillary gland androgen-regulated protein 3A	Smr3a	4	131	p.i.	17.76	18.15	NaN	0.16	—	1.2E-01	2.7E-01
Glia-derived nexin	Serpine2	1	4	p.i.	NaN	NaN	14.52	0.58	3.42	5.2E-01	4.9E-02

NOTE. The number in the columns with color code is mean intensity of proteins (log2 intensity based absolute quantitation) as described by the dot size in Figure 2*D*. The ratio is the fold change of the respective protein in V/M or GF mice compared with untreated (ctrl) mice. The *P* value is the significance level of the abundance difference. Color code: red = high intensity; green = low intensity.
a.p., aspartyl protease; c.p., cysteine protease; iBAQ, intensity-based absolute quantitation; m.p., metalloprotease; NaN, not detected; s.p., serine protease; t.p., threonine protease.